"Study, fabrication and characterization of solar cells based on a-Si:H films deposited by plasma on plastic substrates"

Presented by

Carlos Alberto Ospina Ocampo

A thesis submitted in partial fulfillment of the requirements for the degree of

Ph. D. in Electronic Sciences

at the

National Institute for Astrophysics, Optics and Electronics

June 2018

Tonantzintla, Puebla

Advisors:

Ph. D. Andrey Kosarev, INAOE

and

Ph. D. Ismael Cosme, INAOE

Agradecimientos

Agradecido inmensamente con el Dr. Andrey Kosarev por haberme permitido trabajar con él y por todo lo que de él aprendí, no solo para la culminación del presente trabajo sino también para el resto de la vida.

Agradezco al Dr. Ismael Cosme Bolaños, quien fue mi coasesor, por haber sido un ayudador en el camino. Le admiro por sus extensos conocimientos y la manera rápida de proponer soluciones.

Muchas gracias al Consejo Nacional de Ciencia y Tecnología (CONACyT) por la beca que me fue concedida con N° 377297 y también a la secretaría de energía por el proyecto SENER-CONACYT-INAOE N° 152244.

Muchas gracias a los administrativos, profesores y personal técnico del INAOE por haberme hecho todo fácil y agradable durante este estudio.

Gracias a los doctores que conformaron mi jurado: Dr. Oleksander Malik, Dr. Mario Moreno Moreno, Dr. Svetlana Mansurova, Dr. Israel Vivaldo de la Cruz y al Dr. Carlos Zúñiga Islas.

Mis agradecimientos también son para el personal de laboratorio que me ayudó: Adrián Itzmoyotl con quien compartí momentos fuera del instituto y lo propio de la fabricación con los equipos PECVD y Sputtering. Victor Aca quien me colaboró con depósitos de metales. Armando Hernandez por su ayuda con litografía. Rebeca Lugo y Leticia Tecuapetla por las mediciones en los equipos AFM. Cabe mencionar también a Ignacio Juárez, Juan Alvarez y a Netzahualcoyotl Carlos.

Un agradecimiento especial para Hiram Martínez por su apoyo durante mi trabajo.

Abstract

In this work, plastic substrates PEN, Kapton Polyimide and Teflon were characterized by means of the atomic force microscopy (AFM) technique. Parameters such as maximum height of peaks and width of defects were analyzed. Regions free of defects of these surfaces were also analyzed and the most relevant statistical parameters were determined, such as the RMS roughness, the average height, skewness and kurtosis. In addition to the morphological characterization, spectral measurements were made on the plastic substrates. It was observed that the Teflon substrate has greater optical transmission in the UV spectral region compared to PEN, and exhibits greater transmission in the visible spectrum compared with PEN and Kapton.

p-i-n structures were fabricated on plastic and glass substrates, and the evolution of the morphology in the different layers that make up the p-i-n structure was investigated. The study showed that the morphological characteristics of the surfaces depend on the material used as a substrate, as well as the type of the deposited layers. In addition, treatments with argon (Ar) plasma were studied to improve the adhesion of polymers and AZO films on plastic substrates. The optimal conditions that we found were the following: Power of 30 W, pressure equal to 0.3 Torr and time of 6 minutes. The treatment is the same if done at 110 ° C or at room temperature.

Planarization study of surface defects was carried out on flexible substrates. The study was characterized by AFM and transmittance. Fabrication and characterization of completely inorganic flexible solar cells and some hybrids were carried out. The performance of the solar cells was evaluated through J-V performance curves under AM1.5 illumination.

The discussions carried out during this work allow to formulate the following conclusions: PEN substrates are optimal for the fabrication of flexible photovoltaic devices, because their morphological characteristics (RMS and average height) of underlying films improve as a traditional p-i-n structure is deposited, in addition, these substrates are compatible with fabrication processes with deposition temperatures below 200 ° C. Teflon substrates have a high potential for application in photovoltaic structures due to their high transmittance in the visible (94%), however, Its high density of morphological defects and poor adherence limits its application as a substrate in this type of applications. Finally, in this work, sufficient justification for the use of Kapton as a substrate in photovoltaic devices was not found. Although Kapton has the best initial morphological characteristics, the evolution of morphology of the p-i-n structure changes from lower to higher roughness, affecting the formation of the p-i-n structure. On the other hand, its transmittance in the visible is not optimal for photovoltaic applications.

Resumen

En este trabajo se caracterizaron superficies de sustratos plásticos PEN, Kapton Poliimida y Teflón por medio de la técnica de microscopía de fuerza atómica (AFM). Parámetros como altura máxima de picos y ancho de defectos se analizaron. Regiones libres de defectos de estas superficies también fueron analizadas y se determinaron los parámetros estadísticos más relevantes como son la rugosidad RMS, la altura promedio, "skewness" y curtosis. Además de la caracterización morfológica, mediciones espectrales fueron realizadas sobre los sustratos plásticos. Se observó que el sustrato Teflón posee mayor transmisión óptica en la región espectral UV en comparación con PEN, y exhibe mayor transmisión en el espectro visible comparado con PEN y Kapton.

Se fabricaron estructuras p-i-n sobre sustratos de plástico y vidrio, y se investigó la evolución de la morfología en las diferentes capas que conforman la estructura p-i-n. El estudio mostró que las características morfológicas de las superficies dependen del material usado como sustrato, así como del tipo de las capas depositadas. Además, se estudiaron tratamientos con plasma de argón (Ar) para mejorar la adhesión de polímeros y películas de AZO sobre sustratos plásticos. Las condiciones óptimas que encontramos fueron las siguientes: Potencia de 30 W, presión igual a 0.3 Torr y tiempo de 6 minutos. El tratamiento sirve igual si se hace a 110°C o a temperatura ambiente.

Estudio de planarización de defectos superficiales fue llevado a cabo sobre sustratos flexibles. El estudio se caracterizó por AFM y transmitancia. Se realizó fabricación y caracterización de celdas solares flexibles completamente inorgánicas y algunas híbridas. El rendimiento de las celdas solares fue evaluado a través de curvas de rendimiento J-V bajo iluminación AM1.5.

Las discusiones llevadas a cabo durante este trabajo permiten formular las siguientes conclusiones: Los substratos PEN son óptimos para la fabricación de dispositivos fotovoltaicos flexibles, debido a que sus características morfológicas (RMS y altura promedio) de películas subyacentes mejoran conforme se deposita una estructura tradicional p-i-n, además estos sustratos son compatibles con procesos de fabricación con temperaturas de deposito menores a 200 °C. Los sustratos de Teflón presentan un alto potencial para su aplicación en estructuras fotovoltaicas debido a su alta transmitancia en el visible (94%), sin embargo, su alta densidad de defectos morfológicos y poca adherencia limita su aplicación como sustrato en este tipo de aplicaciones. Por último, en este trabajo no se encontró justificación suficiente para el uso de Kapton como sustrato en dispositivos fotovoltaicos. A pesar de que Kapton presenta las mejores características morfológicas iniciales, la evolución de morfología de la estructura p-i-n cambia de menor a mayor rugosidad, afectando la formación de la estructura p-i-n. Por otro lado, su transmitancia en el visible no es óptima para aplicaciones fotovoltaicas.

CONTENT

CHAPTER 1

1. INTRODUCTION

1.1 Background and justification

This work is development in the framework of the SENER-CONACyT project No. 152244: "PV Solar cells based on Germanium – silicon deposited by PECVD on flexible substrates" with aim of development flexible solar cells and related devices deposited at low deposition temperature compatible with flexible plastic substrates.

The development of flexible electronics goes back to the 60's. The first arrangements of solar cells were made for thinning the crystalline silicon wafer cells up to approximately 100 μm and so assembling them on plastic substrate to give them flexibility [1, 2]. At the beginning of the 80's, p^+ -i - n^+ a-Si:H/ITO solar cells were fabricated on plastics by Okinawa et al. [3-5]. Okinawa and his co-workers also studied the flexibility of their solar cells. Meanwhile, roll-to-roll manufacturing of a-Si: H solar cells on flexible steel [6] and organic polymer [7] substrates was introduced. At the present time, new technologies have been development with promising applications in flexible electronics i.e. organic electronics. However, there still exist some technological challenges to overcome related to the deposition of thin films at low temperature compatible with plastic materials as substrate. In this new context, this work is focused in the study and fabrication of solar cells on plastic substrates and the effect of the morphological characteristics of these substrates on the structure of the devices. More specifically, we have studied the morphological characteristics of the plastic substrates, plasma treatment to enhance adhesion of polymer thin films and the planarization of defects on the plastic substrates via buffer thin films. The results of these approaches were used to fabricate thin films solar cells on flexible and plastic substrates and evaluate their technological potential.

1.2 General Objective and task

The objective of this work is to investigate fabrication process of solar cell based on active a-Si:H thin film deposited by PECVD at low deposition temperature on plastic substrates.

In order to reach the general objective, the task was performed:

1. Study of morphological defects of plastic substrates and their effects on the morphology of the following thin films in p-i-n structures.

2. Study of plasma treatments on plastic substrates to enhance adhesion of thin films deposited by low temperatures process.

3. Deposition and characterization of buffer thin films deposited at low temperatures on plastic substrates and their effect on the planarization of surface defects of the substrates.

4. Fabrication and characterization of flexible solar cells based on active a-Si:H thin film deposited by PECVD at low deposition temperature on plastic substrates.

1.3 Thesis organization

This work is organized as follows: Chapter 2 deals with the analysis of literature of materials used in flexible electronics, some materials for contacts, PECVD for flexible electronics and amorphous silicon deposited at low temperature. The methodology for fabrication and characterization of devices is given in Chapter 3. Chapter 4 presents the results of the study of morphology and defects in p-i-n structures deposited on glass and plastic substrates. It also presents what happens with plasma treatment to improve the adhesion of the Teflon substrate, as well as planarization of plastic substrates. In addition to the above, performance curves (J-V) of different p-i-n structures (inorganic and hybrid) are shown in this chapter. In Chapter 5, results are discussed and compared between them and with data available in literature. Finally, research work summary and conclusion are given in Chapter 6.

CHAPTER REFERENCES

[1] Crabb RL, Treble FC (Mar 25, 1967) Thin silicon solar cells for large flexible arrays. Nature 1223–1224

[2] Ray KA (Jan, 1967) Flexible solar cell arrays for increased space power. IEEE Trans Aerosp Electron Syst v AES-3, n 107–115

[3] Okaniwa H, Nakatani K, Asano M, Yano M, Hamakawa Y (1982) Production and properties of a-Si:H solar cell on organic polymer film substrate. In: Conference record of the sixteenth IEEE photovoltaic specialists conference – 1982, San Diego, CA, USA, Sep. 27–30, San Diego, CA, USA, 1982, pp 1111–1116

[4] Okaniwa H, Nakatani K, Yano M, Asano M, Suzuki K (1982) Preparation and properties of a-Si:H solar cells on organic polymer film substrate. Jpn J Appl Phys 21:239–244

[5] Okaniwa H, Nakatani K (1983) Flexible substrate solar cells. In: Hamakawa Y (ed) JARECT vol. 6. Amorphous Semiconductor Technologies & Devices. Ohusha, Tokyo, pp 239–250

[6] Nath P, Izu M (1985) Performance of large area amorphous Si-based single and multiple junction solar cells. In: Rec 18th IEEE Photovoltaic Specialists Conference. Las Vegas, NV, Oct 21–25, p 939

[7] Yano M, Suzuki K, Nakatani K, Okaniwa H (1987) Roll-to-roll preparation of a hydrogenated amorphous silicon solar cell on a polymer substrate. Thin Solid Films 146:75–81

CHAPTER 2

2. ANALYSIS OF LITERATURE

The development of flexible electronics goes back to the 60's. The first arrangements of solar cells were made of thin crystalline silicon wafer cells (approximately 100 μm) and assembling them on plastic substrate to give them flexibility [1, 2]. In those days hydrogenated amorphous silicon solar cells were fabricated on flexible metal and polymers substrates, due to their low deposition temperature. At the beginning of the 80's, p^+ -i - n^+ a-Si:H/ITO solar cells were made on plastics by Okaniwa et al. [3-5]. Okaniwa and his co-workers also studied the flexibility of their solar cells. Meanwhile, roll-to-roll manufacturing of a-Si: H solar cells on flexible steel [6] and organic polymer [7] substrates was introduced. At present, a-Si: H solar cells are manufactured by roll-to-roll processes. Within large-area flexible electronic structures, substrates play an important role. To manufacture flexible electronic structures, all components should be bending to some degree without losing their functions.

2.1 Materials for flexible solar cell.

Substrate: There are two basic approaches to employee for flexible electronics: (1) Transfer and bonding of the complete circuits to a flexible substrate and (2) circuit fabrication directly on the flexible substrate. Often flexible substrates are not fully compatible with the planar silicon micro manufacturing processes. Direct manufacturing, in our case, can occur with amorphous semiconductors because they can be grown on "foreign" substrates and achieve a compromise between device performance and low process temperatures tolerated by polymeric substrates. Then, flexible substrates have some requirements:

- **Optical properties:** In the case of solar cells, high transmittance allows the passage of photons to reach the cell.
- **Surface roughness:** For thin films of the flexible devices, electrical characteristics are more sensitive to surface roughness. High roughness in short distance must be avoided, but over long distance it is acceptable. Plastic substrates can be rough only in long distance.

- **Thermal and thermo mechanical properties:** The working temperature of the substrate, for example the glass transition temperature (T_g) of a polymer, must be compatible with the maximum temperature of the manufacturing process. Thermal mismatch between films from the device and substrate can cause the films to break during the thermal cycle associated with manufacturing.
- **Chemical properties:** The substrate must not release contaminants and must be inert against chemicals in the manufacturing process.

Table 2.1 shows the typical properties of materials used in flexible applications (metals, polymers and flexible glass). Plastic substrates are highly flexible, can be economical and allow roll-to-roll processing, however, they are thermally and dimensionally less stable than glass substrates and are easily permeated by oxygen and water. The glass transition temperature, compatible with the process temperature of the device is essential, but a high value of T_g is not enough. The dimensional stability and a low coefficient of thermal expansion (CTE) are also important factors [9].

Table 2.1. Properties of substrates used in flexible electronics [8].

Property	Unit	Glass (1737)	Plastics (PEN, PI)	Stainless steel (430)
Thickness	μm	100	100	100
Weight	g/m^2	250	120	800
Safe bending radius	cm	40	4	4
Roll-to-roll processable?	–	Unlikely	Likely	Yes
Visually transparent?	–	Yes	Some	No
Maximum process temperature	°C	600	180, 300	1,000
CTE	ppm/°C	4	16	10
Elastic modulus	GPa	70	5	200
Permeable to oxygen, water vapor		No	Yes	No
Coefficient of hydrolytic expansion	ppm/%RH	None	11, 11	None
Prebake required?	–	Maybe	Yes	No
Planarization required?	–	No	No	Yes
Buffer layer required? Why?	–	Maybe	yes: adhesion, chemical passivation	yes: electrical insulator, chemical passivation
Electrical conductivity	–	None	None	High
Thermal conductivity	W/m·°C	1	0.1–0.2	16
Plastic encapsulation to place electronics in neutral plane	Substrate thickness	5×	1×	8×
Deform after device fabrication	–	No	Yes	No

A large decoupling of CTEs along with a high temperature during manufacturing can break a device film [10]. Plastic substrates with CTE below 20 ppm / ° C are preferred as substrates for silicon-based device materials.

Candidate polymers for flexible substrates include (1) semicrystalline thermoplastic polymers: polyethylene terephthalate (PET) and **polyethylene naphthalate** (**PEN**), (2) non-crystalline thermoplastic polymers: polycarbonate (PC) and polyethersulphone (PES), and (3) High T_g materials: polyarylates (PAR), polycyclic olefin (PCO), and **polyimide** (**PI**). PC, PES, PAR and PCO they are optically clear and have high Tg compared to PET and PEN, but their CTEs are 50 ppm / ° C or higher, and their chemical resistance to the process is poor. Much research has been carried out with PET, PEN and PI with their low magnitude CTEs, namely 15, 13 and 16 ppm / ° C, respectively, and acceptable resistance against process chemicals. PET and PEN have high transmittance (> 85%) in the visible. They absorb little water (~ 0.14%), and their process temperatures are between 150 - 200 ° C. In contrast, PI has high Tg (~ 350 ° C), but is opaque absorbing in blue, and absorbs as much as 1.8% moisture [11, 12].

Contact/electrodes [32]: The materials that serve as electrodes are typically metallic; meanwhile, thin-film solar cells require electrodes that are transparent electric conductors. Generally, metal oxides [13-15] have been used to serve as electrodes in solar cells. The first transparent conductive oxide (TCO), CdO, was reported by Baedeker in 1907 [16]. For several years TCOs were a unique option used as transparent contacts in optoelectronics applications due to their transparency in visible range ($0.4 < \lambda < 0.7$ μ) and low resistivity ($R\square < 100$ Ω/sq). TCOs can be deposited as thin films by techniques as chemical vapor deposition (CVD), pulsed laser deposition (PLD), spray pyrolysis and sputtering. There are a large number of studies with a widely background about the development of this technology and film properties [34]. However, to fabricate transparent contacts compatible with flexible substrates, it is necessary to achieve good optoelectronic properties at low process temperatures (< 200 °C). To reach this goal, the approach followed by the researchers has been: 1) to modify the standard deposition methods, 2) to

propose new techniques of deposition, or most recently 3) to propose new materials with fabrication methods at room temperature i.e. organic based materials.

Sputtering method has been modified to achieve TCOs with high transmittance and low resistivity at low temperature deposition. ITO (In_2O_3) films deposited by roll-to-roll sputtering at low substrate temperature < 50 °C show sheet resistance of 47.4 Ω/sq and a transmittance of 83 %. On the other hand, AZO films have been extendedly studied as alternative to ITO films due to their stability, high transmission, high conductivity, lower cost and lower deposition temperature in comparison to ITO films (AZO films - $R\square \sim 8.5$ Ω/sq and $T_{avg} = 84.44$ % @ $T_d = 200$ °C on glass). ZnO/Al (AZO) films were co-deposited using pulsed-direct current (DC)-magnetron reactive sputtering processes at 188°C using "softpower". The obtained ZnO:Al films show a sheet resistance about $R\square \sim 13$ Ω/sq and a transmittance of ~85 %.

Recently with the introduction of organic materials and new technologies, new options have been studied for substitution of traditional TCOs to overcome some disadvantages as low transmission in blue region, high cost, complex high vacuum process, mechanical characteristics and scarcity. PEDOT:PSS has been one of the most investigated organic material as alternative to TCOs, the polymer has shown higher transparency and conductivity than traditional ITO contacts. Additionally, PEDOT:PSS can be deposited by dispersion in water with compatibility with large area, flexible and low-cost substrates.

TCO materials used as front electrodes exhibit optimal electrical and optical properties during plasma deposition [17]. Aluminum-doped zinc oxide (AZO) and ITO are commonly used as front contact in single solar cell devices. On the other hand, back electrode is used as back reflectors to promote light trapping by reflecting long wavelength into the absorber layer [19].

Table 2.2. Reflectance of back contact materials [18].

Contact	Reflectance a-Si:H/metal contact
Al	0.70
Ag	0.94
Ti	0.22

Table 2.2 summarizes the reflectivity for different back electrode configuration.

2.2 Technology of fabrication for flexible solar cells based on a-Si:H.

Plasma enhanced chemical vapor deposition (PECVD) has reached the versatility to deposit not only amorphous silicon but also silicon materials in their entire range of structure: nanostructured, microcrystalline and epitaxial crystalline silicon. The optoelectronics properties of these materials depend upon deposition parameters such as: pressure, flow rate, deposition temperature, power and excitation frequency. One of the main characteristics of the PECVD technique to take advantage for actual applications, is the relative low temperature process in the range of 100 – 300 °C. It was general think that reduction of temperature below 200° C leads to the increase of dangling bonds (defects) and results in films with electronic properties that are generally poor. However, it has been found that thermal energy reduction can be compensated by other parameters fabrications i.e. increasing ion bombardment. Low-temperature (LT) a-Si:H and LT nanocrystalline (nc) Si:H has been optimized at 120 °C and 75 °C [14].

Roll-to-roll PECVD process is naturally associated with flexible electronics [20]. Roll-to-roll manufacturing of solar cells has the advantage of its reduced cost. Amorphous silicon solar cells have already been manufactured on polyimide sheets [21] by using this process. Other configurations, mainly, cluster semi-industrial PECVD systems has been used successfully to fabricate flexible and large-area modules [25].

In traditional PECVD, substrate temperature T_S is in the range 200-300°C. Reducing this temperature below 150 ° C leads to change in the deposit mechanisms. The concentration of defects (dangling Si bonds) increases, the concentration of di- and polyhydride-bonded hydrogen in the films increases, the density of the mass decreases, and the efficiency of doping drops [42]. Films have low mass density and high charge trapping, and their

electronic properties are usually poor. This change is attributed to the reduced surface mobility of the radicals that build the film due to lower thermal energy on the growing surface [43]. The loss of thermal energy is compensated using "soft" ion bombardment (H^+, He^+) with energy less than 50 eV, or producing exothermic chemical reactions [24, 43]. Continuing this approach, the deposition parameters can be adjusted at low T_S to increase the surface energy and thus facilitate growth conditions like those at higher T_S without overheating the substrate.

The properties of a-Si:H deposited by PECVD at different temperatures are presented in Table 2.3.

Table 2.3. The properties of a-Si:H deposited at 300, 120, and 75◦C

	Deposition temperature		
Parameter	300°C	120°C	75°C
Dark conductivity (σ_{300}), Ω^{-1} cm^{-1}	10^{-10}	4×10^{-11}	9×10^{-11}
Optical gap (E_g), eV	1.75	1.92	1.90
Urbach slope (E_0), meV	–	50	–
Hydrogen concentration (C_H), %	~10	10.9	9.5
Microstructure parameter $R = SiH_n/(SiH+SiH_n)$	<0.1	~0	~0

The films have dark conductivity below $10^{-10}\Omega^{-1}cm^{-1}$, optical bandgap between 1.7 and 1.9 eV, Urbach parameter 50 meV, hydrogen concentration 10 at.%. As shown in the table 2.4, a-Si:H films deposited at low temperatures have good properties for electronic device applications [25, 26].

Work done previously at INAOE

The present work concentrates in the fabrication of structures p-i-n at low temperature. This type of structures has different layers stacked and it is necessary that the films integrated to the devices comply with requirements included in what is known as "device quality" films. Table 2.6 shows the properties of films deposited at low temperature, as well as some data obtained in previous research conducted by Hiram Martínez. The most

relevant parameters when evaluating semiconductor films with "device quality" are dark conductivity σ_{dark}, fermi energy E_F, photoconductivity Urbach energy E_{PC}^{U}, and $\sigma_{ph}/\sigma_{dark}$ ratio.

The intrinsic films used in this work accomplished device quality film characteristics by comparing dark conductivity, $\sigma_{ph}/\sigma_{dark}$ ratio and Urbach energy. The activation energy value of our film is 0.76, which is close to 0.8 eV and the product $\mu\tau$ is one third of the minimum required value.

Table 2.4. Properties of films deposited at low temperature.

Type of Film	Td (°C)	Vd (Å/s)	Eu/E_{PC}^{U}	σ_{dark} ($\Omega^{-1}cm^{-1}$)	$\sigma_{ph}/\sigma_{dark}$	Ea (meV)	E_F (meV)	$\mu\tau$ ($10^{-7}\ cm^2/V$)	Ref.
Device quality	>200	-	<47	$<5\times10^{-10}$	$>2\times10^{4}$	0.8	-	≥ 1 (600 nm)	[37]
Intrinsic	100	2.42	76	$<5\times10^{-7}$	-	-	-	0.3	[38]
Intrinsic	150	1.84	57	-	-	-	-	4	[38]
Intrinsic	160	0.6	45	7×10^{-11}	-	0.76	0.68	0.38 (633 nm)	[30]
n-type	150	-	-	1×10^{-3}	-	-	-	-	[38]
n-type	150	-	-	4.2×10^{-3}	-	195	-	-	[39]
n-type	160	0.52	-	3.5×10^{-3}	-	0.32	0.32	-	[30]
p-type	160	0.80	-	2×10^{-6}	-	0.36	0.36	-	[30]
p-type	125	0.92	-	2×10^{-7}	3.4	-	-	-	[40]
p-type	180	-	-	$\sim2\times10^{-6}$	-	~0.43	-	-	[41]

Even so, our films can be considered like those found in devices manufactured at low temperature (<200 ° C) reported in literature. For our doped films, σ_{dark} has good values like those of literature. N-type films exhibit conductivities of the order of $10^{-3}\ \Omega^{-1}cm^{-1}$, values also observed in [38] and [39].

2.3 Performance characteristics of flexible solar cells.

Performance characteristics of flexible solar cell based on a-Si:H are compared in table 2.5.

Table 2.5. Characteristics of PV devices fabricated by low temperature PECVD (literature).

Configuration	Intrinsic material	Substrate	Td (°C)	Voc (V)	Jsc (mA/cm^2)	FF	Textured?	Frontal contact	PCE (%)	Ref.
n-i-p	a-Si:H	PEN	150	0.640	7.38	0.53	No	AZO	1.65	[44]
n-i-p	a-Si:H	PEN	150	0.700	9.66	0.56	No	Al/Cr	3.8	[45]
p-i-n	a-Si:H	PET	110	0.900	8.8	0.61	No	AZO	4.9	[46]
p-i-n	a-Si:H	PEN	150	0.770	8.4	0.61	No	ZnO (sputtering)	3.99	[47]
n-i-p	a-Si:H	PEN	<200	0.888	11.3	0.67	Yes	ZnO LPCVD	6.6	[48]

In Ref. [44] The development of amorphous silicon thin film photovoltaic modules fabricated at 150 ° C over PEN is reported. The configuration of their cells differs from ours because they use the n-i-p configuration and use a combination of Al with another metal as the top electrodes. In Ref. [46] the authors fabricate their solar cells at a temperature of 110 ° C and use PET as a substrate. The configuration chosen in [46] is the same as the one with which we decided to work (p-i-n). In this work they strive to improve efficiency by achieving 4.9% in their devices. In Ref. [47] the fabrication of thin-film silicon p-i-n solar cells at low temperatures was investigated. The authors studied the effect of silane diluted by hydrogen on the performance characteristics of solar cells. They achieved efficiencies of 3.99% in their cells deposited on plastics. In Ref. [48] was used a-Si:H as the base material for thin-film solar cells in the n-i-p configuration with substrate PEN as substrate. The authors of this work texturized the surfaces of the substrates to have better light scattering and investigated the correlation between substrate morphology and Jsc. Their “flat” solar cells achieved an efficiency of 6.6%.

References

[1] Crabb RL, Treble FC (Mar 25, 1967) Thin silicon solar cells for large flexible arrays. Nature 1223–1224

[2] Ray KA (Jan, 1967) Flexible solar cell arrays for increased space power. IEEE Trans Aerosp Electron Syst v AES-3, n 107–115

[3] Okaniwa H, Nakatani K, Asano M, Yano M, Hamakawa Y (1982) Production and properties of a-Si:H solar cell on organic polymer film substrate. In: Conference record of the sixteenth IEEE photovoltaic specialists conference – 1982, San Diego, CA, USA, Sep. 27–30, San Diego, CA, USA, 1982, pp 1111–1116

[4] Okaniwa H, Nakatani K, Yano M, Asano M, Suzuki K (1982) Preparation and properties of a-Si:H solar cells on organic polymer film substrate. Jpn J Appl Phys 21:239–244

[5] Okaniwa H, Nakatani K (1983) Flexible substrate solar cells. In: Hamakawa Y (ed) JARECT vol. 6. Amorphous Semiconductor Technologies & Devices. Ohusha, Tokyo, pp 239–250

[6] Nath P, Izu M (1985) Performance of large area amorphous Si-based single and multiple junction solar cells. In: Rec 18th IEEE Photovoltaic Specialists Conference. Las Vegas, NV, Oct 21–25, p 939

[7] Yano M, Suzuki K, Nakatani K, Okaniwa H (1987) Roll-to-roll preparation of a hydrogenated amorphous silicon solar cell on a polymer substrate. Thin Solid Films 146:75–81

[8] Cannella V, Izu M, Jones S, Wagner S, Cheng IC (Jun, 2005) Flexible stainless-steel substrates. Inf Display24–27

[9] MacDonald WA (2004) Engineered films for display technologies. J Mater Chem 14:4–10

[10] Cheng IC, Kattamis A, Long K, Sturm JC, Wagner S (2005) Stress control for overlay registration in a-Si:H TFTs on flexible organic-polymer-foil substrates. J Soc Inf Disp 13(7): 563–568

[11] MacDonald BA, Rollins K, MacKerron D, Rakos K, Eveson R, Hashimoto K, Rustin B (2005) Chapter 2: Engineered films for display technologies. In: Grawford GP (ed) Flexible Flat Panel Displays. John, England, pp 11–33

[12] http://www.Dupont.com/kapton/products/H-78305.html

[13] Ginley DS, Bright C (2000) Transparent conducting oxides. MRS Bull 25:15–18

[14] Lewis BG, Paine DC (2000) Applications and processing of transparent conducting oxides. MRS Bull 25:22–27

[15] Paine DC, Yeom HY, Yaglioglu B (2005) Chapter 5: Transparent conducting oxide materials and technology. In: Grawford GP (ed) Flexible Flat Panel Displays. Wiley, England, pp 80–98

[16] Baedeker K (1907) U¨ ber die elektrische Leitfa¨higkeit und die thermoelektrische Kraft einiger Schwermetallverbindungen. Ann Phys 22:749–766

[17] A. V. Shah *et al.*, "Thin-film silicon solar cell technology," *Prog. Photovoltaics Res. Appl.*, vol. 12, no. 23, pp. 113–142, Mar. 2004.

[18] J. Kanicki, *Amorphous and Microcrystalline Semiconductor Devices: Materials and device physics*. Artech House, 1992.

[19] A. Banerjee and S. Guha, "Study of back reflectors for amorphous silicon alloy solar cell application," *J. Appl. Phys.*, vol. 69, no. 2, pp. 1030–1035, 1991.

[20] Ghosh AP, Gerenser LJ, Jarman CM, Fornalik JE (2005) Thin-film encapsulation of organic light-emitting devices. Appl Phys Lett 86:223503

[21] Takano A, Tabuchi K, Uno M, Tanda M, Wada T, Shimosawa M, Sakakibara Y, Kiyofuji S, Nishihara H, Enomoto H, Kamoshita T (2006) Production technologies of film solar cell. Mater Res Soc Symp Proc 910:0910-A25-04

[22] Fruehauf N, Chalamala BR, Gnade BE, Jang J (2004) Flexible Electronics 2004 – Materials

and Device Technology, vol 814. Materials Research Society Symposia Proceedings, Pittsburgh, PA, USA

[23] Reuss R et al. (2005) Macroelectronics: Perspectives on technology and applications, Proc IEEE 93:1239

[24] Sazonov A, Nathan A (2000) 120◦C Fabrication technology for a-Si:H thin film transistors on flexible polyimide substrates, J Vac Sci Technol A18:780–782

[25] Nathan A, Striakhilev D, Servati P, Sakariya K, Sazonov A, Alexander S, Tao S, Lee CH, Kumar A, Sambandan S, Jafarabadiashtiani S, Vygranenko Y, Chan IW (2004) a-Si AMOLED display backplanes on flexible substrates, In: Fruehauf N, Chalamala BR, Gnade BE, Jang J (eds) Flexible Electronics 2004 – Materials and Device Technology, vol 814. Materials Research Society Symposia Proceedings, Pittsburgh, PA, USA, pp I3.1.1– I3.1.12

[26] Sazonov A, Striakhilev D, Nathan A (2000) Materials optimization for TFTs fabricated at low temperature on plastic substrate, J Non-Cryst Solids 266–269:1329–1334

[27] N. Shibata, K. Fukuda, H. Ohtoshi, J. Hanna, S. Oda, and I. Shimizu, Mater. Res. Soc. Symp. Proc. 95, 225 (1987)

[28] X. Liao, H. Povolny, P. Agarwal, and X. Deng, “Raman and IR study of narrow bandgap a-SiGe and _c-SiGe films deposited using different hydrogen dilution” it in Photovoltaic Specialists Conference, 2002. Conference Record of the Twenty-Ninth IEEE Volume , pp. 1150 - 1153, (19-24 May 2002).

[29] W. Beyer and H. Wagner, “The role of hydrogen in a-Si:H results of evolution and annealing studies” *Journal of Non-Crystalline Solids*; Vol. 59-60, pp. 161-168, (1983).

[30] H. Martínez, “Study of optoelectronic characteristics of photovoltaic devices based on Si and related films deposited by RF glow discharge at low temperatura in a multichamber system,” INAOE, 2018.

[31] J. S. Cho, S. Baek, S. H. Park, J. H. Park, J. Yoo, and K. H. Yoon, “Effect of nanotextured back reflectors on light trapping in flexible silicon thin-film solar cells,” *Sol. Energy Mater. Sol. Cells*, vol. 102, pp. 50–57, 2012.

[32] Andrey Kosarev, Ismael Cosme, Svetlana Mansurova, Antonio J. Olivares and Hiram E. Martinez (July 12th 2017). Hybrid Silicon-Organic Heterojunction Structures for Photovoltaic Applications, Optoelectronics Sergei Pyshkin, IntechOpen, DOI: 10.5772/67565. Available from: https://www.intechopen.com/books/optoelectronics-advanced-device-structures/hybrid-silicon-organic-heterojunction-structures-for-photovoltaic-applications

[33] I. Cosme, A. Kosarev, S. Mansurova, A.J. Olivares, H.E. Martinez, A. Itzmoyotl. Hybrid photovoltaic structures based on amorphous silicon and P3HT:PCBM/PEDOT:PSS polymer semiconductors. Organic Electronics. 2016;**38**:271- 277.

[34] K.A. Nagamatsu, S. Avasthi, J. Jhaveri, J.C. Sturm. A 12% efficient silicon/PEDOT:PSS heterojunction solar cell fabricated at <100°C. IEEE Journal of Photovoltaics. 2014;**4**(1):260-264.

[35] E.L. Williams, G.E. Jabbour, Q. Wang, S.E. Shaheen, D.S. Ginley, E.A. Schiff. Conducting polymer and hydrogenated amorphous silicon hybrid solar cells. Appl. Phys. Lett. 2005;**87**:223504-223506.

[36] K.-H. Choi, J.-A. Jeong, J.-W. Kang, D.-G. Kim, J.K. Kim, S.-I. Na, D.-Y. Kim, S.-S. Kim, H.-K. Kim. Characteristics of flexible indium tin oxide electrode grown by continuous roll-to-roll sputtering process for flexible organic solar cells. Solar Energy Materials & Solar Cells Materials. 2009;**93**:1248-1255.

[37] Jef Poortmans and Vladimir Arkhipov, J. Poortmans, and V. Arkhipov, *Thin Film Solar Cells Fabrication , Characterization and Applications*, vol. 1. 2006.

[38] C. Koch, M. Ito, and M. Schubert, “Low-temperature deposition of amorphous silicon solar cells,” *Sol. Energy Mater. Sol. Cells*, vol. 68, no. 2, pp. 227–236, 2001.

[39] G. Hou, G. Li, J. Fang, C. Wei, X. Zhang, and Y. Zhao, “Inclusion of nanometer-sized silicon crystallites in n-layer for open circuit voltage enhancement in amorphous silicon solar cell,” *Sol. Energy Mater. Sol. Cells*, vol. 128, pp. 126–130, 2014.

[40] J. Ni *et al.*, “Low temperature deposition of high open-circuit voltage (>1.0V) p–i–n type amorphous silicon solar cells,” *Sol. Energy Mater. Sol. Cells*, vol. 95, no. 7, pp. 1922–1926, Jul. 2011.

[41] A. Hadjadj, P. St’ahel, P. Roca I Cabarrocas, V. Paret, Y. Bounouh, and J. C. Martin, “Optimum doping level in a-Si:H and a-SiC:H materials,” *J. Appl. Phys.*, vol. 83, no. 2, pp. 830–836, 1998.

[42] Robertson J (2000) Deposition mechanism of hydrogenated amorphous silicon, J Appl Phys 87:2608–2617

[43] Perrin J (1995) Reactor design for a-Si:H deposition, In: Bruno G, Capezzuto P, Madan A (eds) Plasma Deposition of Amorphous-Based Materials, Academic Press, San Diego, CA, pp 177–241

CHAPTER 3

3. METHODOLOGY

3.1 Semiindustrial "Mvsystem" PECVD cluster system

Plasma enhanced chemical vapor Deposition or PECVD is a fabrication technique that provides acceptable deposition rates, good quality film, conformability and low deposition temperatures. A plasma source is used together with a thermal source to give the energy that is needed for chemical reactions to produce radials and deposition. When we talk about plasma, reference is made to partially ionized gases. By supplying additional plasma energy to the gases, the reactions required for the deposition can occur at much lower temperatures than those that are needed when only thermal energy is provided in traditional CVD process. With this method is also possible to achieve deposition at room temperature, but the common thing is to deposit in the range 200-350 ° C [3.1]. The PECVD technique enables changing film properties (density, composition, stress, etc.) and the adjustment of these properties by changing fabrication parameters. This is mainly due to the nonequilibrium nature of this deposition process. Nevertheless, this can also lead to undesirable compositions or properties in films. PECVD is a variant of CVD. CVD allows to make a solid film on a substrate due to the reaction of chemical species in vapor phase. A typical equipment configuration for PECVD is shown in the figure 3.1.

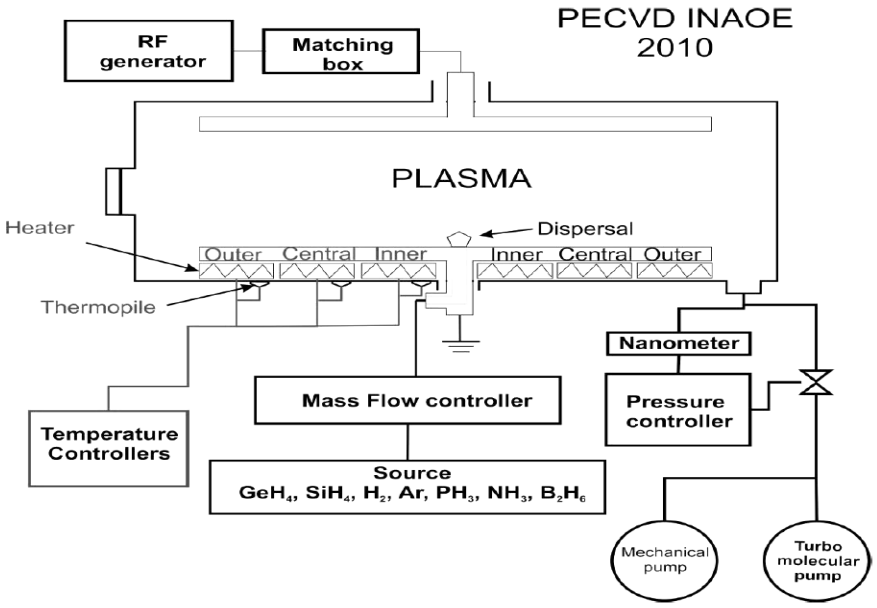

Figure 3.1. Schematic representation of a PECVD system.

In deposition enhanced by plasma, energetic species are used to create films on top of the substrate. The substrates are in the electrode of the lower plate. Through a heater positioned below the electrode, the heat is transferred to the samples. The reactant gases, for example, silane and oxygen are introduced through input lines. A glow discharge or plasma is maintained between the lower and upper electrodes. Plasma is formed by applying a high electric field to a low pressure gas (Between 50 mTorr and 5 Torr), creating ions and free electrons. Plasma is maintained when high-energy electrons collide and ionize atoms and molecules.

Reactant gases dissociate and ionize in a variety of species due to interactions with high-energy electrons in the plasma. Among the species mentioned are molecules (or atoms) ionized and excited, neutral molecules, as well as ionized and neutral fragments of separated or dissociated molecules, including free radicals. The latter are electrically neutral species that have incomplete bonds; That is, Radicals have unpaired electrons. SiO and SiH_3 are examples of such radicals in the plasma deposition. Such species are very reactive and with other species are absorbed on the surface of the samples, migrate, interact, they rearrange and recombine chemically to create the film. There is also bombardment of ions and electrons from the plasma on the surface of the samples. A potential difference exists between the plasma and the surface of the samples in the radio frequency plasma systems, where the surface of the sample is electrically negative with respect to the plasma. Thus, positive ions are accelerated to the surface of the samples. Such bombardment of ions and electrons transfers more energy to the species on the surface, breaking chemical bonds, which contributes to the different processes and reactions on the surface. The result of plasma-induced fragmentation, the generation of free radicals and the bombardment of ions, is that processes and deposition on the surface can occur at much lower temperatures than in systems without plasma. Finally, the byproducts of the deposition reactions are desorbed and removed through the vacuum line.

Deposited films by PECVD have good coverage and filling of non-planar topography, like deposition made at higher temperatures in systems without plasma. This is attributed to the long-range order surface diffusion, enhanced by the most energetic species and by the bombardment of ions.

Experimental deposition system.

In this work, a cluster system tool for Research and Development from "MVSystem, Inc." is used to deposit silicon, silicon carbide, silicon-germanium, and germanium hydrogenated film; Cluster tools reduce cross- and ambient- contamination in multi-layer thin film structures due to the Isolation and Transportation Zone (ITZ) with a robotic arm. It is possible to control the system by a computer based Human Machine Interface (HMI). Also, a Load Lock (LL) chamber with a single substrate capability provides entire isolation with the room environment. Four chambers constitute the cluster system: ITZ: Chamber for isolation and transportation (Gas: N), PL1: Load and Lock chamber (Gases: N), PL2: PECVD Chamber for p type materials (Gases: SiH4, GeH4, CH4, H2, B2H6, Ar) PL3: Sputtering Chamber for electrode materials (Gas: Ar; Ag and AZO targets), PL4: Chamber for intrinsic materials (Gases: SiH4, GeH4, H2, Ar) and PL7: Chamber for n type materials (Gases SiH4, GeH4, H2, PH3, Ar)

3.2 Flexible materials substrates

The substrates used in the present work are: Dupont Teijin Teonex Q51 (PEN - Polyethylene Naphthalate), Dupont Kapton Polyimide and Dupont Teflon FEP. Some desirable characteristics of the substrates are: compatible with the manufacturing process, high thermal stability so they should retain their shape. During deposition process, dielectric constant must be uniform and isotropic, and, they must have a high chemical resistivity. Where possible, their surfaces must be free of defects. Something desirable is that they have good adhesion with metals and that they could be low cost.

Dupont Kapton Polyimide is a heat-resistant polymer. Polyimide has found applications in the field of aerospace, defense, optoelectronics and is used in electroluminescent devices. It is possible to say for this material that it has good electrical properties, good mechanical resistance and is resistant to solvents. It is a stable polymer up to a temperature of 440 ° C in a nitrogen atmosphere.

Dupont Teijin Teonex Q51 is a plastic with a high glass transition temperature and water permeability. It has found use in digital radiography applications, cell phone screens, within the automotive industry and in wearable solar cells. This material allows freedom of design and other characteristics such as resistance to multiple thermal cycles up to 200 ° C, vacuum cycles to $1 \times 10^{-8}\ Torr$, solvents such as acetone and plasma processes with

several chemicals such as O_2, O_3, Cl, NH_3, H_2. Also, PEN can be used at temperatures as high as 240 ° C.

Dupont Teflon FEP is chemically resistant, resists almost all aggressive products, has a working temperature in the range -200 to + 260 ° C, it is not affected by being outdoors, or exposure to the sun and does not absorb moisture.

3.3 Film thickness measurements

The thickness of the films was determined with the surface profile measuring system (profilometer) "DEKTAK V 200 - Si". Prior to measuring the thickness usually lithographic processes are performed and plasma etching to make geometric patterns on films.

3.4 Optical Transmission Characterization

The transmittance measurements allow to obtain values of optical constants. The optical transmittance gives information of the range in the spectrum where the film has a percentage of transparency or opacity. The refractive index $n(\lambda)$, optical band gap E_g and the absorption coefficient $\alpha(\lambda)$ are parameters that are extracted as a function of wavelength [3.2]. The optical model for the study of fabricated samples is shown in figure 3.2.

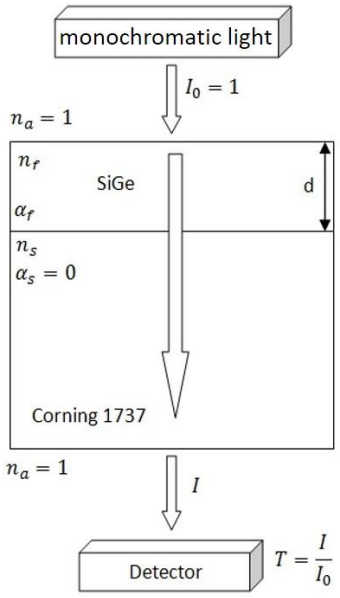

Figure 3.2. Thin film system deposited on transparent substrate of finite thickness.

The film has a complex refractive index $n = n_f + ik$, where n_f is the refractive index of the film and k the extinction coefficient. The thickness of the film is denoted in Figure 3.4 by the letter "d". From the ratio $k = \frac{\alpha\lambda}{4\pi}$ the absorption coefficient of the film can be calculated α_f. The refractive index of the substrate is n_s and its absorption coefficient is $\alpha_s \approx 0$. The refractive index of the air is $n_a = 1$.

Figure 3.3 shows a typical example of the absorption spectrum obtained after light transmission measurements. Region A is the Tauc region, where the spectral shape can be approximated by equation 3.1 and is attributed to the optical electronic transition between extended valence and conduction bands. In a Tauc model:

$$\alpha(h\upsilon)h\upsilon \propto \left(h\upsilon - E_g\right)^2 \quad (3.1)$$

Where E_g is the optical energy gap (or Tauc). The Tauc model conveniently displays the optical absorption spectrum of a material. This graph shows the amount $h\upsilon$ on the horizontal axis and the quantity $(\alpha h\upsilon)^r$ on the vertical axis, where α is the absorption coefficient of the material. The value of the exponent r indicates the nature of the transition, for example $r = 0.5$ is for indirect transitions in crystalline semiconductors. The Tauc graph has a distinctive linear regime which shows the principle of absorption. Thus, extrapolating this linear region to the x-axis gives the energy of the optical band gap of the material. In figure 3.5 it can be seen that E_g changes to lower energies as the deposition temperature increases. This change may be correlated with the decrease in bound hydrogen content of the film [3.3]. Region B is known as the Urbach region and has an exponential form given by equation 3.2.

$$\alpha(h\upsilon) = \alpha_g \exp\left[\frac{h\upsilon - E_g}{E_U}\right] \quad (3.2)$$

Where E_U it's called the Urbach energy. This region can be described in terms of a transition between a band tail state and an extended band. The C region can be attributed to optical transitions involving structural defects.

The transmittance values are between 0 and values close to unity ($0 \leq T < 1$). As shown in Figure 3.4, the transmittance is the ratio between transmitted intensity and source, logically there are losses due to light that is absorbed in the film and the substrate (It is desirable that the substrate absorb little light). There are also losses due to reflections at the interfaces air - glass, glass - air. It is not common for the transmittance values at their maximums to reach unity, the maximum transmission can be approximated as shown in equation 3.3

$$T_M \approx (1-R)^2 \quad (3.3)$$

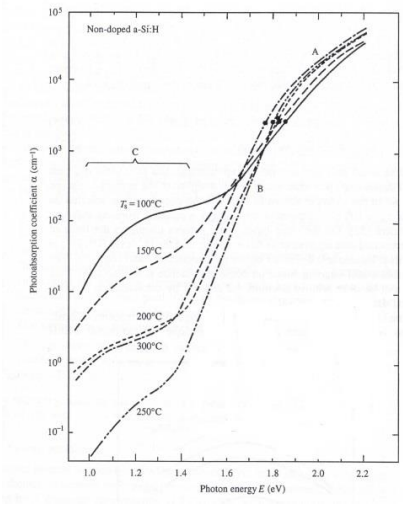

Figure 3.3. Light absorption spectrum of un-doped a-Si: H prepared at different substrate temperatures [3.3].

Being R the reflectance term or reflection coefficient, given by the refractive index of the substrate and the surrounding medium as shown in equation 3.4.

$$R = \left(\frac{n_s - n_{medio}}{n_s + n_{medio}}\right)^2 \quad (3.4)$$

As an example, the Corning 1737 has the refractive index in a range between 1.5023 and 1.5247 for the wavelengths in the range 1541 and 435.8 nm respectively. The index of the surrounding medium, which for this case is air has the value of 1, thus T_M will have the values between 0.9155 and 0.9210.

3.5 Atomic Force microscopy (AFM)

Atomic Force Microscopy is a technique for imaging the surface of a sample by monitoring the deflection of a cantilever, which has a tip in vertical position. The cantilever interacts with the atoms of the sample surface. The deflection of the tip is monitored by an optical system that sends a beam of laser light towards the end of the cantilever where the tip is located and the reflection of the beam reaches a sensor (photodiode) that registers the change of the vertical position of the cantilever as a variation of the position of the laser beam on the positioning sensor. When the tip approaches the sample, the tip stops being in its equilibrium position thanks to the force experienced by the tip atoms closest to the sample. The tip is curved to the sample when the force is attractive and is curved in the opposite direction when the force is repulsive. The relationship between force and distance in the interaction between atoms of the sample and atoms of the tip is described by a force-distance curve. Statistical parameter related to morphology of the films are:

Surface height distribution function: The meaning of the height distribution function $p(h)$ is that the probability of a height between h y $h + dh$ at any point on the surface be $p(h)dh$. The distribution p(h) is normalized and shown in equation 3.5

$$\int_{-\infty}^{+\infty} p(h)dh = 1 \quad (3.5)$$

This distribution function provides a complete specification of $h(r)$ in a position **r**. The most used distribution is Gaussian and is shown in equation 3.6

$$p(h) = \frac{1}{\sqrt{2\pi}\omega} \exp\left(-\frac{h^2}{2\omega^2}\right) \quad (3.6)$$

Where ω is given in units of length and depends on the technique used to determine the roughness parameters.

RMS roughness: Also known as moment of order 2 is shown in equation 3.7.

$$R_q = \omega^2 = m_2 = \int_{-\infty}^{+\infty} h^2 p(h)dh \quad (3.7)$$

Where R_q is the RMS roughness or the width of the interface. In this case it is equal to the standard deviation since h¯=m_1=0. R_q describes the fluctuations of surface heights

around an average surface height. Generally, as R_q becomes larger, the surface is rougher while the other roughness parameters do not change.

Average roughness: It is defined as the arithmetic average of h and is represented in equation 3.8

$$R_a = \int_{-\infty}^{+\infty} |h - \bar{h}|\, p(h)dh \quad (3.8)$$

For the same height distribution $R_a \propto R_q$. Taking the Gaussian height distribution as an example $R_a = R_q\sqrt{\frac{2}{\pi}}$. With $\bar{h}$ and R_q is enough to characterize the surface roughness for most cases.

Skewness: This parameter defines the "lack of symmetry" of the surface height, its symbol is γ_3 and it is shown in equation 3.9

$$\gamma_3 = \frac{1}{\omega^3}\int_{-\infty}^{+\infty} h^3 p(h)dh \quad (3.9)$$

The value of Skewness is dimensionless. It is a measure of the symmetry of a distribution around a medium surface level. If its magnitude is positive, means that the farthest points are upwards from the medium surface level and if the magnitude of skewness is negative, then these points are down from the middle level.

Kurtosis: It is known as fourth order moment and defines the kurtosis of the surface height γ_4, its mathematical formula is given below:

$$\gamma_4 = \frac{1}{\omega^4}\int_{-\infty}^{+\infty} h^4 p(h)dh \quad (3.10)$$

The kurtosis is dimensionless. It is a measure of the sharpness of the height distribution function. Kurtosis describes the randomness of the surface profile relative to that of a Gaussian distribution surface, which has a kurtosis of 3.0. For $\gamma_4 < 3$, distribution presents soft peaks, and $\gamma_4 > 3$ the distribution presents sharp peaks, as shown in figure 3.4.

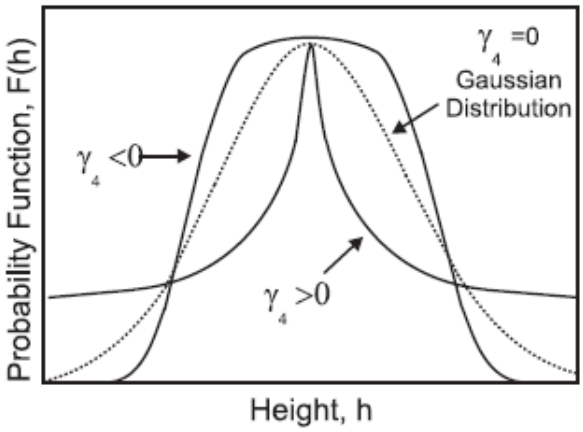

Figure 3.4. Surface height distribution functions with different kurtosis values.

Lateral correlation length: Or simply known as correlation length, ξ, is defined as the value of the out-of-phase length, at which the autocorrelation function falls to 1 / e of its value when it is in phase and is shown in equation 3.11

$$R(\xi) = \frac{1}{e} \quad (3.11)$$

Where ξ defines a representative lateral dimension of a rough surface. When the distance between two points on the surface is equal to or less than ξ, the heights in these two points are considered correlated. But if such separation is much greater than ξ, then it can be said that the heights at such points are independent.

Morphology measurements in this work were performed by an "easyScan 2.3" microscope from "Nanosurf Inc." at the beginning and later with "NTEGRA" scanning probe microscope (SPM) from "NT-MDT". Statistical analysis of surface morphology was applied to AFM images by means of "Igor Pro" and "Image Analysis" software from "WaveMetrics, Inc" and "NT-MDT" respectively. A scanning area of 2x2 μm2 was selected as representative film area.

3.6 Device performance characterization

The performance of photovoltaic devices can be known by means of current-voltage measurements under illumination conditions. Parameters that can be found with this technique can be the short circuit current density (Jsc), open circuit voltage (Voc), efficiency (η) and fill factor (FF). By obtaining a current-voltage curve, it is also possible to determine other characteristics of the fabricated device such as series and shunt resistance values.

In this work, photovoltaic structures fabricated and subjected to measurements are evaluated according to an equivalent circuit model, which is shown in figure 3.5.

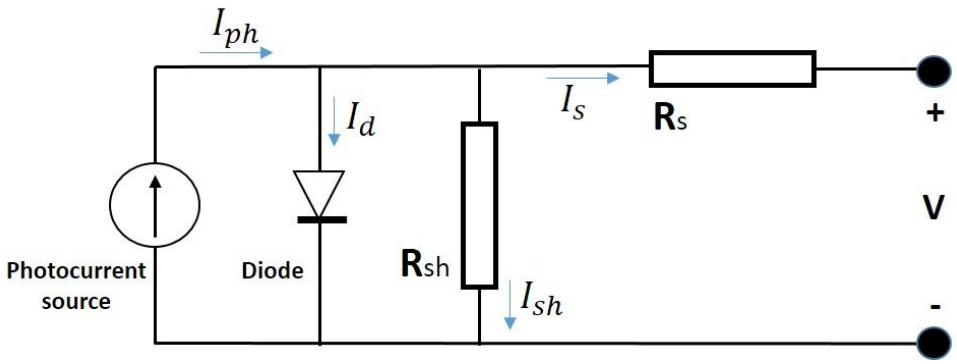

Figure 3.5. Circuit model representing a photovoltaic structure.

The circuit of Figure 3.5 is composed of a photocurrent source, a diode, a shunt resistor and a series resistance. The photocurrent source represents the photogenerated current in the volume of the intrinsic layer. The diode has information related to the quality of the joints in the structure. The shunt resistor is related to short circuits in the contacts with the electrodes, or shorts that arise by pinholes or micro cracks in the joints. The series resistance is physically related to the contact resistance or non-ohmic contacts, the volume resistivity of the intrinsic layer, as well as it is related to spreading resistance in the front interface.

Experimental setup for I(V) measurements under AM 1.5 illumination

Figure 3.8 shows the hardware configuration that allows the realization of current-voltage measurements under AM 1.5 illumination at room temperature.

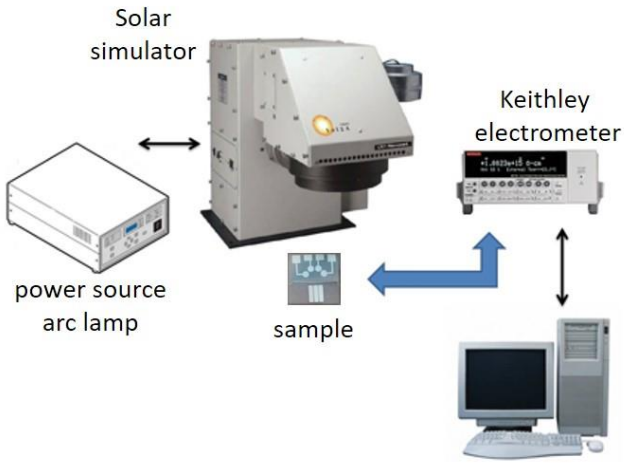

Figure 3.6. Experimental setting for I (V) measurements under AM 1.5 illumination.

The experimental setting consists of a solar simulator, model Oriel 2A class ABA (100 mW / cm2) from "Newport Corp." with its respective power source, an electrometer (Model 6517A) from "Keithley Instrument Inc.", a computer with its GPIB interface to control the electrometer, and micro-probes to contact the pads of the samples. The measurements are done in the DC regime.

3.7 Spectral Jsc device response

With the spectral response, the performance of a photovoltaic device is evaluated according to the wavelength that characterizes the collection of the sun spectrum for conversion of electrical output.

The external quantum efficiency (EQE) is the ratio of the number of electrons in the external circuit produced by an incident photon with a given wavelength (see equation 3.13) [3.5]. The term EQE is also known as the ratio of incident photon to charge carrier efficiency (IPCE) or calibrated spectral response [3.6].

$$IPCE = \frac{J_{sc}}{q\Phi} \quad (3.12)$$

The spectral response determined in this work corresponds to the spectral response of the short circuit current density (JSC) under monochromatic illumination at 0V polarization.

Experimental setup for Jsc spectral measurements

The experimental setup used for JSC spectral measurements in the DC regime. The installation consists of a "Triax 320" monochromator from "Horiba Jobin Yvon Ltd.", an electrometer of "Keithley instruments" model 6517A, a 71938 thermopile sensor from "Thermo Oriel Instruments Inc." as well as xenon and halogen lamps. The lamps are polychromatic light sources, each with a power of 100 W. The monochromatic light beam has a photon flow of $1 \times 10^{16} s^{-1} cm^{-2}$ with resolution 4 nm. Photon flux was calculated from monochromatic intensity measurements with a 71938 thermopile from "Thermo Oriel Instruments Inc." with sensitivity equal to 260 μA / W.

Measurements are made in the wavelength range from 200 to 1200 nm. The measurements were carried out in dark conditions on a table that isolates the vibrations and at room temperature. The system is turned on 30 minutes before measurements to ensure thermal stability.

Spectral response of the optical adjustment is shown in figure 3.9. The intensity of the light beam of the experimental setting was measured with the thermopile 71938 of "Thermo Oriel Instruments Inc.".

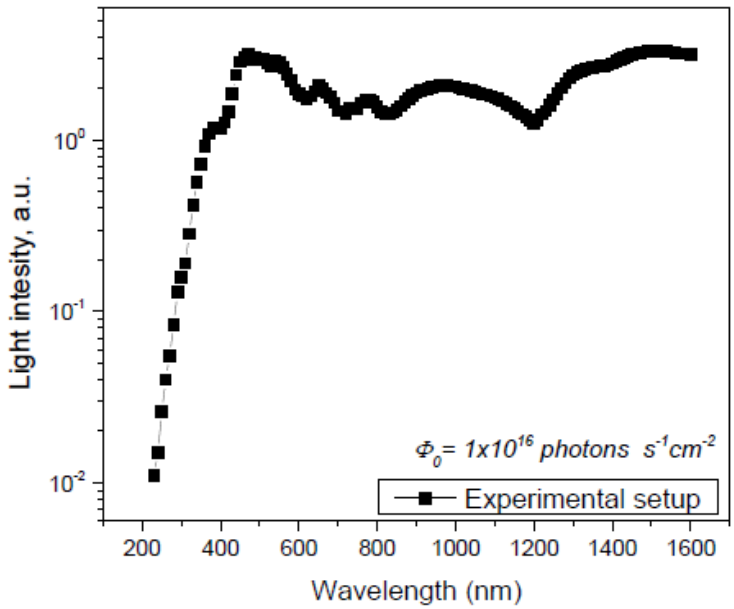

Figure 3.7. Optical adjustment spectral response.
$\Phi_0 = 1.03 \pm 0.15 \times 10^{16}\ photons \cdot s^{-1}cm^{-2}$ at 470 nm.

The spectral response of the samples is obtained by means of equation 3.13.

$$J_{SC}(\lambda)_{\Phi_0-const} = \frac{J_{SC-primary\ data}(\lambda)}{S^{\Phi_0}_{experimental\ setup}(\lambda)} \quad (3.13)$$

Where $J_{SC}(\lambda)_{\Phi_0-const}$ represents the spectral response of the device and S^{Φ_0} to the spectral response of the experimental setting under constant photon flux.

The spectral response is presented as the incident photon-to-electron conversion efficiency (IPCE). Figure 3.10. shows an example IPCE curve where the standardized IPCE was calculated.

$$IPCE[0,1] = \frac{J_{SC}(\lambda)_{\Phi_0-const}}{\Phi(\lambda)} \quad (3.14)$$

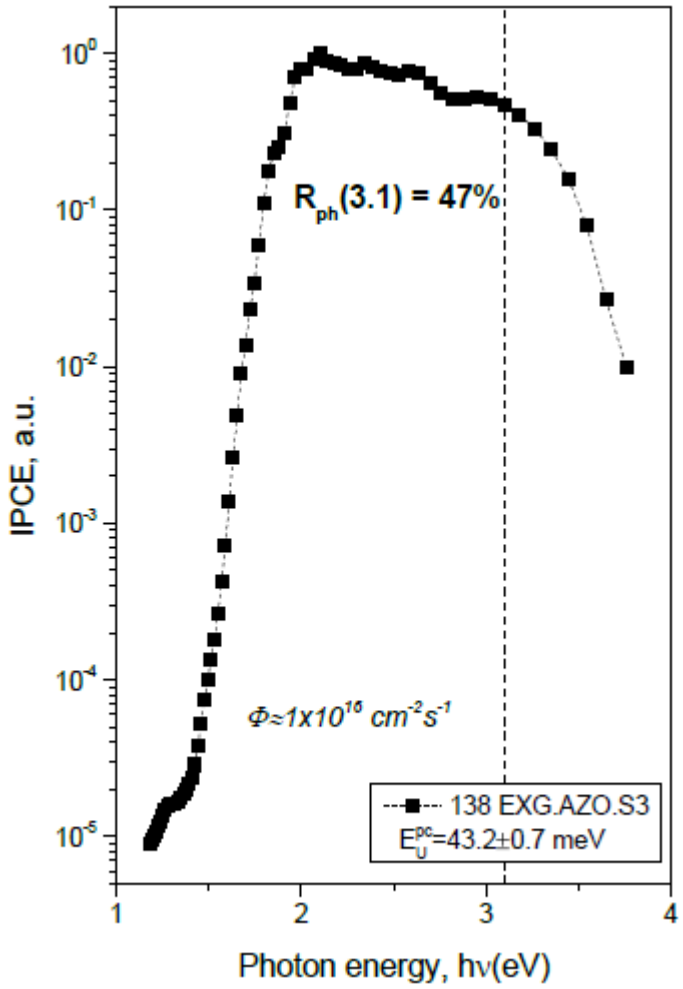

Figure 3.8. Spectral response of a sample calculated at a constant rate of photon flow.

IPCE measurements can give information about the intrinsic layer quality, density of tail states and interfaces formed with the intrinsic semiconductor region. By changing the energy of the incident photons the region where the absorption takes place can be controlled. High-energy photons are absorbed in the active region close to the frontal interface while photons with energy close to E_g are absorbed throughout the active layer.

REFERENCES

[3.1] James D. Plummer, Michael D. Deal, Peter B. Griffin “Silicon VLSI Technology. Fundamentals, practice and modeling”; Prentice Hall, (2000).

[3.2] Sánchez Morales, Liborio “Growth and Characterization of Nano-structured Silicon-Germanium Films deposited by LF PECVD”, [Tesis de doctorado], INAOE, Puebla, 2007.

[3.3] K. Tanaka, E. Maruyama, T. Shimada, H. Okamoto, T. Sato. Amorphous Silicon. John Wiley & Sons 1999.

[3.4] http://inaoe.repositorioinstitucional.mx/jspui/handle/1009/238

[3.5] A. J. McEvoy, L. Castañer, and T. Markvart, *Solar Cells: Materials, Manufacture and Operation*. Academic Press, 2012.

[3.6] G. P. Smestad *et al.*, “Reporting solar cell efficiencies in Solar Energy Materials and Solar Cells,” *Solar Energy Materials and Solar Cells*, vol. 92, no. 4, pp. 371–373, 2008.

CHAPTER 4

4. EXPERIMENTAL RESULTS AND DISCUSSION

4.1 Study of flexible substrates and their morphological effect on p-i-n structure.

In this section is presented a study of morphological characteristics of the interface surfaces to reveal evolution of surface morphology with subsequently deposited films in Si:H p-i-n device configuration on “Corning” and plastic substrates.

4.1.1 Evolution of morphological characteristics of Si:H p-i-n structures deposited by plasma on "corning" substrates.

First, to investigate the effect of growth of p-i-n structures on plastic substrates, the morphological evolution of each layer was studied on glass substrate:

Table 4.1. Deposition conditions of each layer that comprises a p-i-n device deposited on Corning.

Interface	Parameters →	Pressure (Torr)	Time (s)	Flow rate (sccm)			
				SiH_4	PH_3	B_2H_6	CH_4
5C	n-layer	0.55	185	30	0.3	-	-
4C	Intrinsic layer	0.55	8500	10	-	-	-
3C	p-layer	0.69	80	30	-	15	12
2C	Carbon layer	0.69	60	-	-	-	4.5
1C	AZO	Thin Film Devices, Inc. - ≤ 100 Ohms/sq. – 88% @ 550 nm					

Si:H p-i-n device structures were deposited in a cluster tool system with 3 chambers from “M.V.S. Systems. Inc.”, p-, i and n- layer is deposited in p-, i- and n-chamber, respectively, with sample transportation in vacuum to prevent cross contamination. Intrinsic Si:H film was deposited from 10 % SiH_4 + 90 % H_2 mixture, p+ doped layer Si:H(B) from 0.32 % B_2H_6 + 3.64 % CH_4 + 6.43 % SiH_4 + 89.6 % H_2 mixture and n+ doped layer from 0.01 % PH_3 + 9.9 % SiH_4 + 90.09 % H_2 mixture. "Corning" glass coated by the film of Al doped zinc oxide (AZO) was used as substrate with transparent conductive oxide (TCO). Deposition frequency f= 13.56 MHz and power W= 3W.

Deposition conditions with flow rates of silane, diborane, phosphine y methane used in deposition of p-, i- and n-layers and carbon layer are specified for the fabrication process in

table 4.1. In all cases, before the deposition of p-type layer, surface treatment with Ar plasma was conducted. Gas pressure during deposition of p-type layers was P= 0.69 Torr, and that for depositing the intrinsic and n-type layers was P= 0.55Torr. The deposition times shown in table 4.1 are directly related to the thickness of each layer. Figure 4.1 shows the structure fabricated.

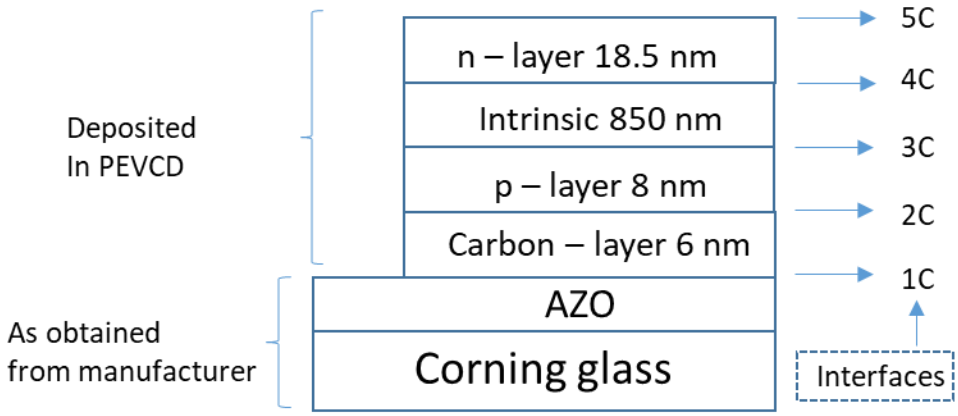

Figure 4.1. Schematic of layered p-i-n device. The numbers are used for identification of surfaces studied by AFM.

The carbon layer had a deposit time equal to 60 seconds, the p-type layer 8 nm. The intrinsic layer is the thickest layer of the structure with a thickness d_i= 850nm and finally the n-layer is deposited with a thickness d_n= 18.5 nm. TCO serves as the bottom electrode and contact and as a transparent window to allow penetration of incident light into the device (typical solar cell).

Experimental characterization of the samples started with AFM measurements of surface morphological characteristics of the substrate. Then morphological characterization was measured after PECVD growth of each layer in p-i-n structure.

AFM characterization was performed with “easyScan2.3” from “Nanosurf”. Surface morphology statistical analysis of the AFM images was carried out with software “Igor Pro” (from “WaveMetrics, Inc.”). The Surface morphology was measured for each layer in the p-i-n structure. Interface 1C (see figure 4.1) corresponds to the boundary between TCO and C-layer, interface 2C to the boundary between C-layer and p-layer, the frontier between p-layer and intrinsic layer is the interface number 3C.

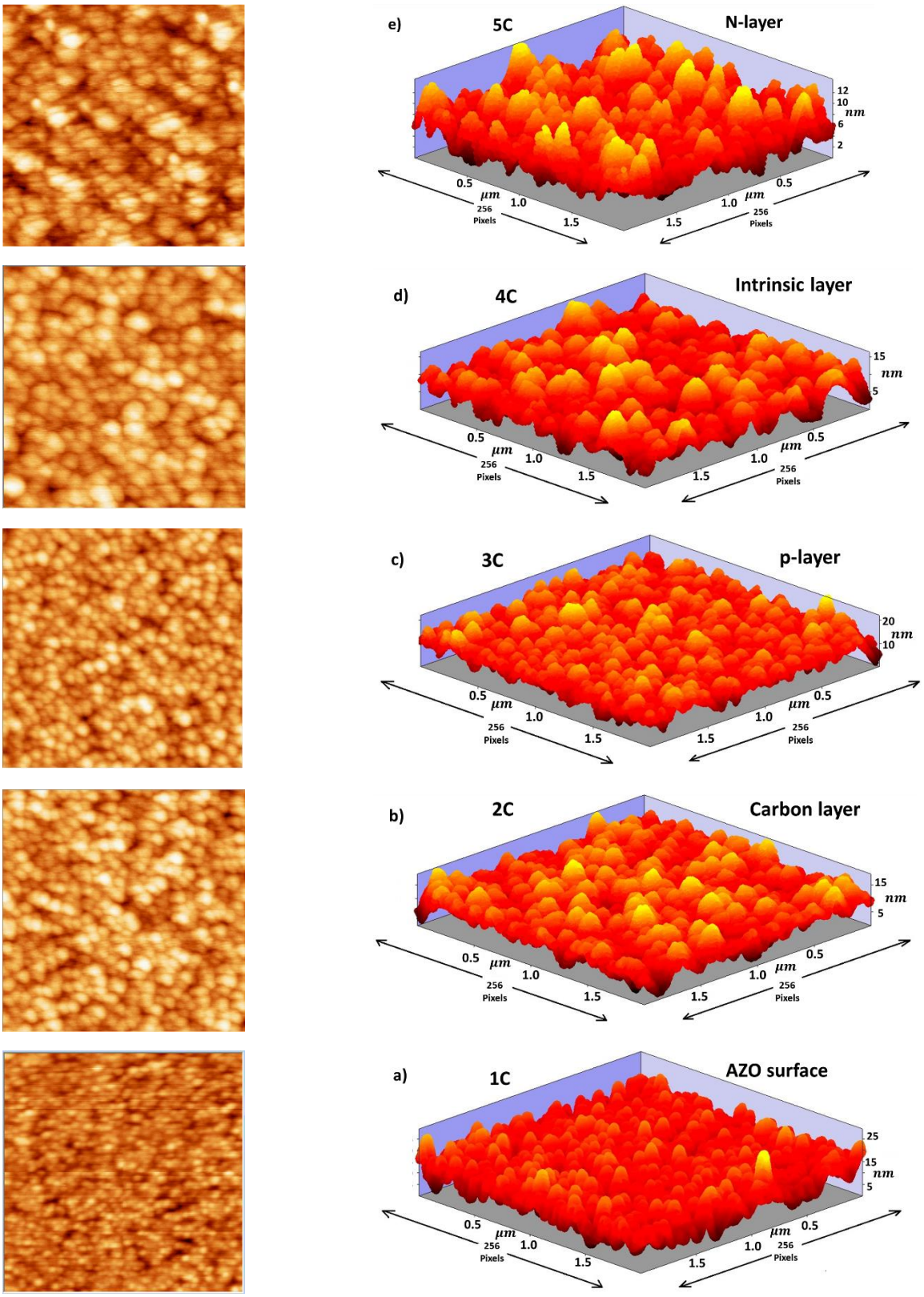

Figure 4.2. AFM images of the different interfaces. 1C: AZO Surface. 2C: Carbon layer. 3C: p-layer. 4C: Intrinsic layer. 5C: n-layer.

The interface 4C is one that formed by the intrinsic layer and n-layer, the last layer studied is the n-layer, which is designated as the interface 5C. AFM images were taken for randomly selected areas, the dimensions of the exploration area are 2x2 μm^2.

Figure 4.2 shows 3D AFM images of each surface of the layers comprising the p-i-n structure fabricated. To facilitate comparison between the different surfaces, the same scale was selected. All the images obtained have a resolution of 256 x 256 pixels. The surfaces are shown from bottom to top i.e. from the lower layer, which corresponds to the surface of glass-AZO to the surface of the n-type layer. The height related morphological characteristics for these samples are presented in Table 4.2. The following statistical characteristics were calculated: the mean height <H>, root-mean-square height RMS, skewness γ_3 and kurtosis γ_4.

Table 4.2. Morphological characteristics of height for interfaces studied in p-i-n structure on Corning.

Interface →	1C	2C	3C	4C	5C
Parameter	AZO	Carbon	p-layer	Intrinsic layer	n-layer
<H> (nm)	12.81	10.02	11.55	10.17	6.86
RMS (nm)	3.14	2.59	2.69	2.46	2.23
γ_3	-0.06	0.08	-0.05	0.14	0.24
γ_4	3.16	2.82	3.03	2.96	2.91

In Table 4.2 the values of the height characteristics are summarized. The average height tends to decrease with the number of layers of the structure (on the AZO surfaces <H> is 12.8 nm and on n-layer surface <H> is 6.86 nm). γ_4 and RMS parameters demonstrate the average height behavior. On AZO surface γ_4 is equal to 3.16 and in n-layer surface takes a value of 2.91 meaning that the form of valleys become smoother in comparison to that described by gaussian formula. Analyzing the values of the skewness (γ_3) can be seen that this parameter shows a minimal change from 1C to 3C interfaces and increases for 4C and 5C interfaces. This means that the morphology in these cases is mostly determined by hills. The value of the RMS roughness in the interface 1C is equal to RMS= 3.14 nm and decreases in the n-layer surface to RMS= 2.23 nm, indicating that the roughness decreases with consequent film depositions.

Figure 4.3 shows a 2D grayscale AFM image that illustrates grain-like structure suggesting importance of lateral characteristics. The hills look darker in the figure. In Figure 4.3 the grain boundaries are indicated for further analysis of lateral characteristics.

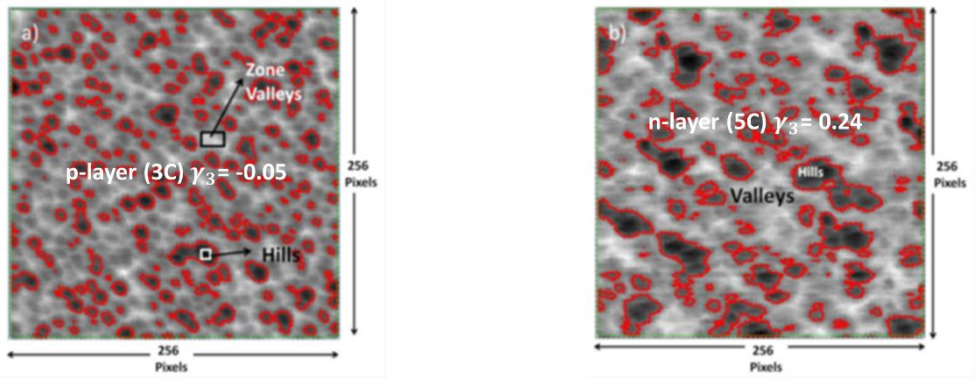

Figure 4.3. AFM images with defined boundaries between valleys and hills, a) interface 3C (p-layer) and b) interface 5C (n-layer).

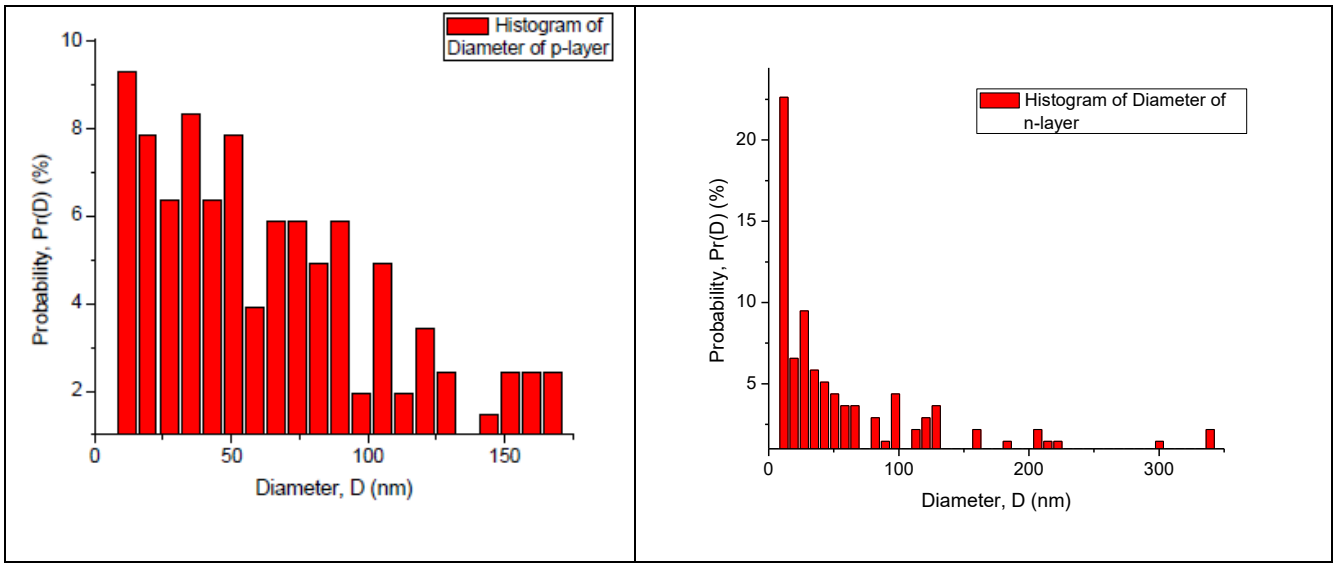

Figure 4.4. Distribution function of probability of grain diameter for the p-layer (left) and n-layer (right).

The boundary definition in this work is based on the optimal threshold level (height or depth), for which the overlap of grains or pores is minimal, then it is possible to identify separate grains and determine lateral morphological characteristics. Figure 4.3, demonstrates an example of the change of morphology with deposition conditions and different beneath surface. Two of the five surfaces studied are displayed in figure 4.3. In the figure 4.3 (a and b) grain boundaries are showed by a red line defining the perimeters of the

grains. Figure 4.4 presents the probability distribution of the diameters Pr(D) = f(D) for the interfaces 3C and 5C (see also images in figure 4.3). Table 4.3 summarizes systematically data on Pr(D) to reveal some trends.

Table 4.3. Morphological lateral characteristics for interfaces studied for p-i-n structure deposited on glass substrate.

Interface →	1C	2C	3C	4C	5C
<D> nm ↓	Probability (%)				
11.7	13.41	15.03	9.31	20.63	22.63
27.3	5.8	7.84	6.37	5.56	9.49
35.1	5.07	7.19	8.33	4.76	5.84
44.85	4.35	5.23	6.37	0.79	5.11
48.75	3.62	3.92	7.84	7.14	4.38
60.45	3.62	2.61	3.92	6.35	3.65
66.3	1.81	5.88	5.88	3.17	3.65
74.1	0.72	5.88	5.88	3.97	0.73

From the table 4.3 and Figure 4.4 it is possible to see that grain diameters near <D>= 11.7 nm have the highest probability reaching a maximum value of Pr= 22.6% on the interface 5C. It means that during growth of intrinsic film there are some preferential conditions for growth of the grains with <D>= 11.7 nm. In table 4.3, it is not given a simple average value because it is not a correct statistical characteristic in this case. Weighted average based on the diameter distribution function describe lateral morphology better. After averaging, values of weighted average are found for each interface and they are shown in figure 4.5.

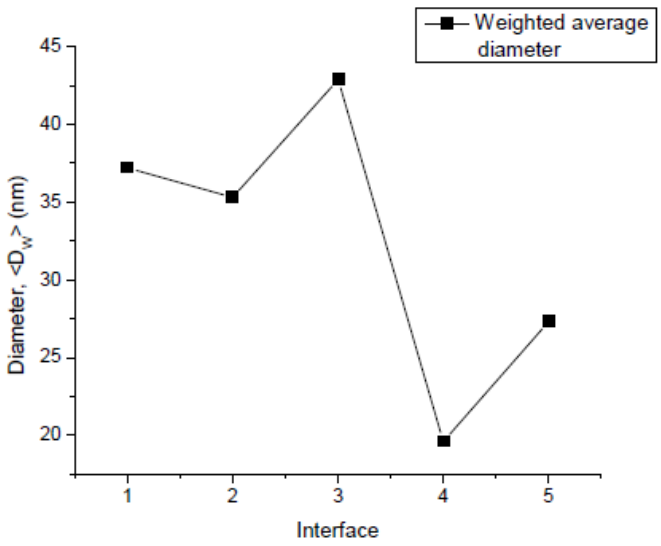

Figure 4.5. Diagram showing the weighted average diameter behaviour through various interfaces.

Weighted average value for the diameter allows to calculate the ratio of height to diameter AR= <H>/<D_W> (known as aspect ratio), where <D_W> is the weighted average diameter. The latter parameter gives further information on the morphology of the layers studied in this work. In Figure 4.6 it is shown a diagram which displays the behavior of aspect ratio for different interfaces.

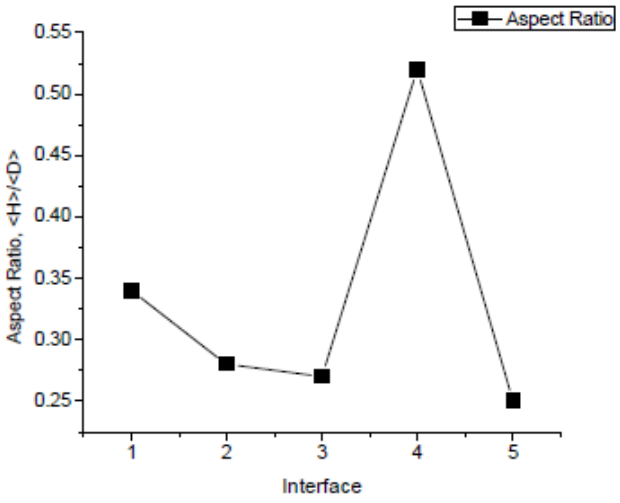

Figure 4.6. Diagram showing behavior of aspect ratio through various interfaces.

In Figure 4.6 the value of the aspect ratio decreases from interface 1 to interface 3, with an increase in interface 4 (surface of the intrinsic layer), and then reaching a minimum of AR in interface 5.

4.1.2 Morphological characteristics of "Corning", Teflon, PEN and Kapton substrates.

Morphological characteristics of substrates is important for this work. It is important to note that these characteristics are not declared by the manufacturer in any case. Table 4.4 shows the morphological characteristics of Corning glass and Figure 4.7 shows a two-dimensional image of an AFM measurement on Corning 1737, a 3D image of the morphology of this glass and a height profile image. The surface of the analyzed glass has a low number of defects.

Table 4.4. Morphological characteristics of Corning substrate.

Substrate	RMS Roughness (nm)	<H> (nm)	γ_3	γ_4
Corning	1.21	4.15	0.47	3.15

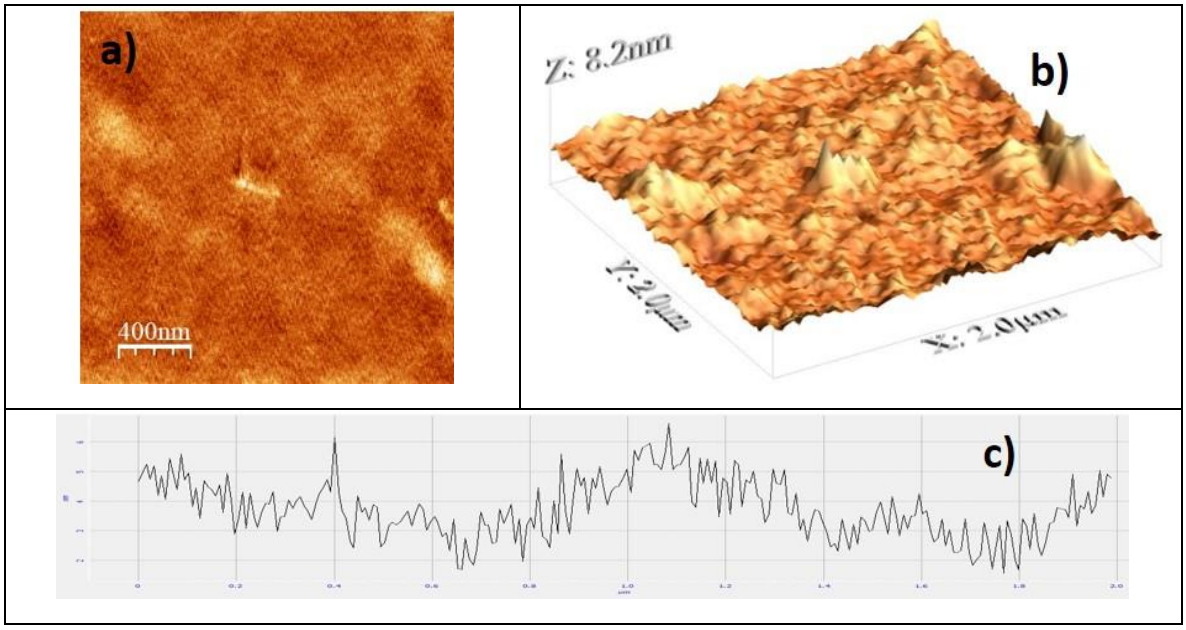

Figure 4.7. Corning substrate a) 2D view. b) 3D view. c) Height profile.

Corning glass has a low roughness RMS = 1.21 nm, its value of kurtosis (γ_4) indicates that on its surface the hills are smooth and its skewness value represents a surface with greater contribution of hills than valleys.

The AFM statistical analysis of Teflon surface is shown in Tables 4.5 and 4.6. Figure 4.8 corresponds to images of morphology data of the Teflon plastic substrate. In a) a two-

dimensional view can be observed which indicates that the Teflon surface is easily scratched.

Table 4.5. Defects in Teflon substrate.

Type	Number	Value
Maximum peak height Sp (nm)	1	53.26
	2	54.40
	3	90.72
Maximum valley depth Sv (nm)	4	52.47
	5	43.83
	6	49.12
Channel width (nm)	4	922
	5	1140
	6	1270

Table 4.6. Morphological characteristics of Teflon substrate.

Substrates	Teflon
LcX (um)	0.2
LcY (um)	0.266
Average diameter (um)	0.248
RMS Height (nm)	7.29
Kurtosis	2.735
Skewness	0.126

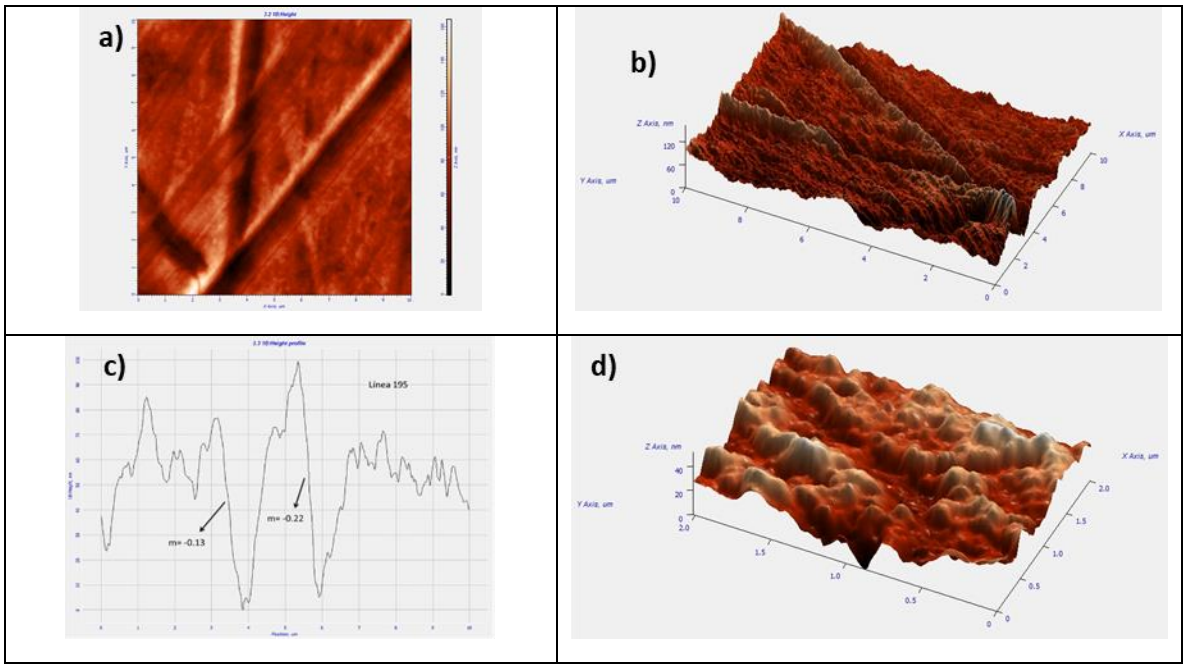

Figure 4.8. Teflon plastic substrate a) 2D view. b) 3D view. c) Height profile. d) 3D view of characteristic morphology section.

In b) it has a corresponding 3D view and clearly shows a very fractured surface that is far from a perfectly flat surface. The image in c) is a cross section showing the height and width of defects. The values of the slopes of each channel were determined, -0.13 and -0.22. In d) there is a 3D view of an area where the defects are not seen, and that surface is referred to as "characteristic".

For characterization of defects on the Teflon surface, 3 parameters were measured, namely, Maximum peak height, maximum valley depth and channel width. The average peak height value is 66.13 nm. The channels have an average depth of 48.47 nm and the width of them is averaged at 1110 nm ($\sim 1 \mu m$). To characterize the morphology of the characteristic surface of the Teflon substrate, the average diameter, rms height, kurtosis, as well as skewness and correlation length values on x and y axes were determined.

Figure 4.9 corresponds to AFM images of the substrate surface PEN. a) and b) are 2D and 3D views respectively. The image in c) is a cross section in the place where the largest defect observed in a) and b) is. The image in d) is of the characteristic surface of the PEN substrate. A visual comparison between Fig 4.8 a) and Fig 4.9 a), as well as Fig 4.8 b) and Fig 4.9 b) shows that there is less area with defects in the PEN sample. A comparison of the "characteristic" AFM images shows that the Teflon peaks are softer than those of PEN.

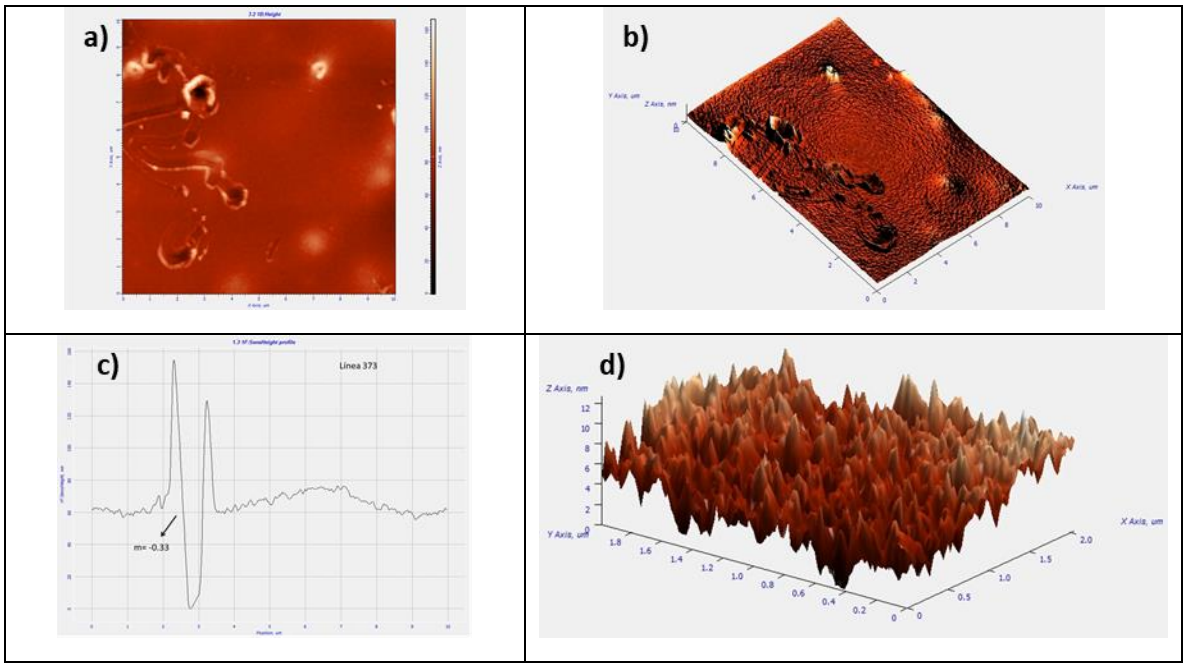

Figure 4.9. PEN plastic substrate. a) 2D view. b) 3D view. c) Height profile. d) 3D view of characteristic morphology section.

It was previously said that the defects had been processed individually for each measured sample. Table 4.8 summarizes the defects that were characterized for the PEN substrate. There are 14 different easily locatable defects to which their width, diameter, height RMS and maximum peak height were determined. The width with smallest magnitude found is 76.7 nm, the largest width was 528 nm and the average value is 205 nm. The smallest diameter found was 221.4 nm, the largest diameter was 1367 nm, the average value being 625 nm. The lowest RMS height found was 4.95 nm, the largest has a magnitude of 28.98 nm and the average value is 12.3 nm. Regarding the maximum peak height parameter, the lowest was 19.02 nm, the highest has a magnitude equal to 113.68 nm and the average value is 51.2 nm.

Table 4.7. Defects in PEN substrate.

Number	Width (nm)	Diameter (nm)	RMS height of the surface (nm)	Maximum peak height (nm)
1	205	815	19.08	72.56
2	138	421	28.98	113.68
3	205.8	633.6	18.31	74.27
4	109.2	439.7	8.98	25.19
5	79.2	292	7.34	53.45
6	153	494	12.03	50.7
7	100.9	335.6	9.43	41.39
8	109	389	9.7	61.08
9	487	1367	4.95	19.02
10	528	1176	7.59	29.38
11	96.8	445	6.14	32.58
12	481	1202	7.83	30.83
13	76.7	522.3	17.42	69.95
14	104	221.4	14.75	42.8

Table 4.8. Morphological characteristics of PEN substrate.

Substrates	PEN
LcX (um)	0.0852
LcY (um)	0.0586
Average diameter (um)	0.102
RMS Height (nm)	1.904
Kurtosis	2.836
Skewness	0.113

Figure 4.10 corresponds to AFM images of the substrate surface Kapton. a) and b) are 2D and 3D views respectively. The AFM statistical analysis of Kapton surface is shown in Tables 4.9 and 4.10.

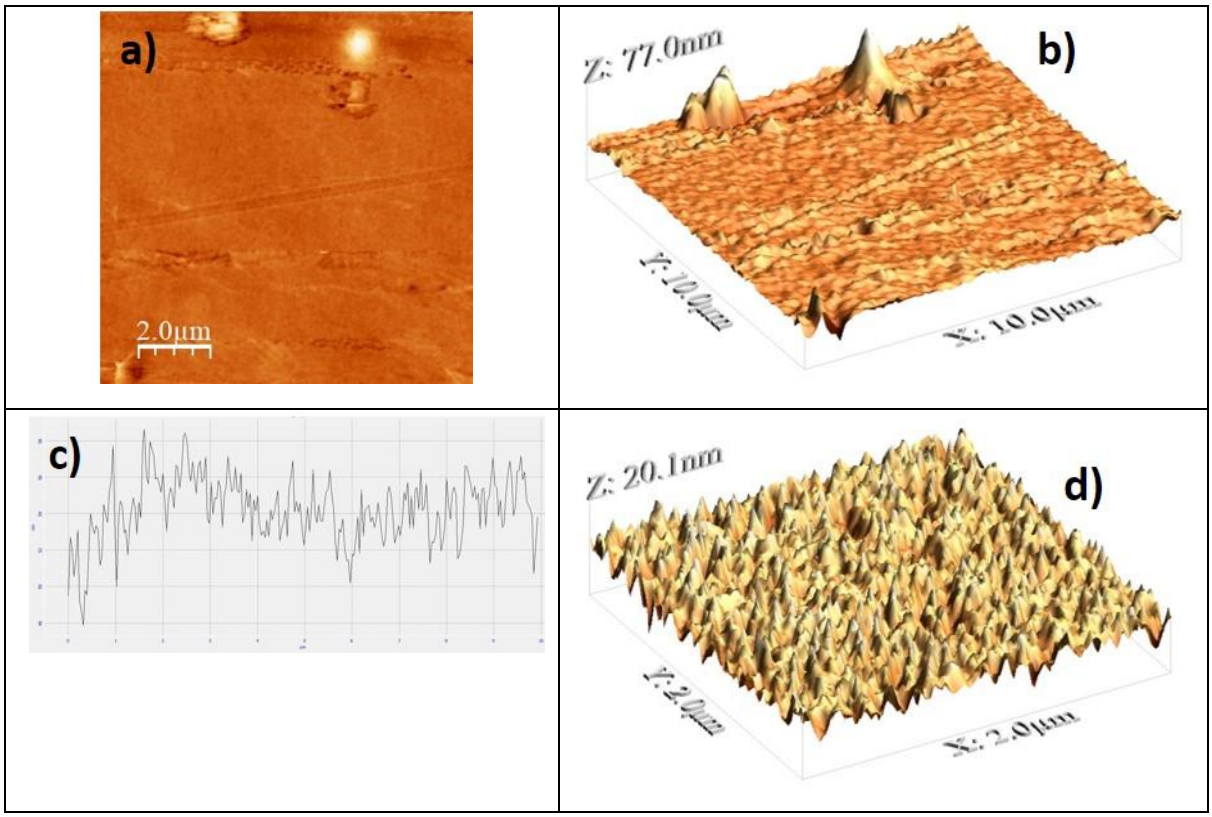

Figure 4.10. Kapton plastic substrate. a) 2D view. b) 3D view. c) Height profile. d) 3D view of characteristic morphology section.

Table 4.9 Defects in Kapton Polyimide substrate.

Number	Width (nm)	Diameter (nm)	RMS height of the surface (nm)	Maximum peak height (nm)
1	170.2	346.4	23.66	83.18
2	135.2	346.4	20.11	74.69
3	156.5	517	10.77	31.39
4	232.1	587.8	11.85	31.13
5	65.3	138.5	6.28	23.43
6	19.6	119.1	4.19	20.68
7	64.4	180.5	4.69	18.79
8	36.3	119.8	10.56	32.7
9	212	841	2.99	10.21

Table 4.10. Morphological characteristics of Kapton polyimide substrate.

Substrates	Kapton Polyimide
LcX (um)	0.119
LcY (um)	0.072
Average diameter (um)	0.105
RMS Height (nm)	1.068
Kurtosis	3.424
Skewness	-0.259

Partial analysis of the morphological characteristics of the Teflon, PEN and Kapton substrates shows that the correlation length values are higher in Teflon (0.2 μm) than in PEN (0.08 μm) or Kapton (0.119 μm), both in the X axis and in the Y axis. The average diameter in Teflon it also has greater magnitude in Teflon (0.248 μm) than in PEN (0.102 μm) or Kapton (0.105 μm). When calculating the average grain diameter for these substrates it was found that there were 110 grains in Teflon, 466 in PEN and 431 in Kapton. The RMS height in Teflon is 7.29 nm, in PEN 1.90 nm and lower in Kapton (1.068 nm).

The kurtosis and skewness parameters have very similar values for both substrates, γ_4(Teflon)= 2.735 and γ_4(PEN)= 2.836, as well as γ_3(Teflon)= 0.126 and γ_3(PEN)= 0.113, respectively. But Kapton exhibits γ_4(Kapton)= 3.424 and γ_3(Kapton)= -0.259. The latter means that the surface of kapton has hills less sharp than the hills of the other two substrates and that it also has a greater contribution of valleys.

Analysis of defects of the different plastics show that the surface of Teflon is the most "defective", observing an average maximum peak height of 66.13 nm with an average width of approximately $1\mu m$. In an intermediate level is PEN with average height values of 51.21 nm and a width of 205 nm, which is 5 times less than that found in Teflon. With the values of defects of smaller magnitude, the Kapton substrate is found, average height 36.24 nm and defect width 121 nm.

These values of defects are consistent with the observed in the laboratory during the fabrication processes. It seems that there is a direct correlation between the quality of adhesion of films deposited on these substrates and the bending temperature.

4.1.3 Evolution of morphological characteristics of Si:H p-i-n structures deposited by plasma on flexible substrates (PEN and Kapton)

In this section is presented a study of morphological characteristic evolution of the substrate surfaces and the substrate surfaces coated with metal and Si:H p-i-n structures, to reveal effect of plastic surface morphology and its evolution with subsequently deposited films including Si:H p-i-n device configuration.

Teflon "FEP 500A", polyimide "Kapton 500 HN" (from "DuPont" Inc.) and PEN (polyethylene naphthalate) "Teonex Q51" (from "Teijin Inc.") were used as substrate materials in this study. Metal electrodes (Ti) were deposited by DC sputtering in the installation from "AJA Int. Inc". Si:H p-i-n layers on plastic coated by Ti were deposited in a cluster tool system with 3 chambers from "MVS system. Inc.", p-, i and n-layer is deposited in p-, i- and n-chamber, respectively, with sample transportation in vacuum to prevent cross contamination. Intrinsic Si:H film was deposited from 10 % SiH_4 + 90 % H_2 mixture, p^+ doped layer Si:H(B) from 0.32 % B_2H_6 + 3.64 % CH_4 + 6.43 % SiH_4 + 89.6 % H_2 mixture and n^+ doped layer from 0.01 % PH_3 + 9.9 % SiH_4 + 90.09 % H_2 mixture. Deposition temperature was T_d= 160° C. RF discharge is excited at frequency f=13.56 MHz and power W= 3W. In table 4.11 flow rates of silane, diborane and phosphine used in deposition of p-, i- and n- layers are specified for the fabrication process. Before to the deposition of p-type layer, treatment with Ar plasma was conducted. The gas pressure during deposition of p-type layers was P=0.69 Torr, and that for depositing the intrinsic and n-type layers was P= 0.55 Torr. Titanium frontal and rear contacts had a thickness of 70 Å. The final structure is represented in Fig. 4.11.

Table 4. 11. Deposition conditions of process 73.

	S_iH_4 (sccm)	B_2H_6 (sccm)	PH_3 (sccm)	Pressure (Torr)
p-layer	30	0.6	-	0.69
i-layer	10	-	-	0.55
n-layer	30	-	0.3	0.55

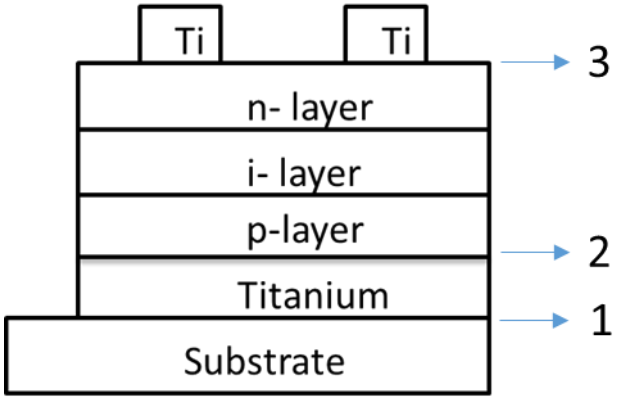

Figure 4.11. Schematic of process No. 73.

Experimental characterization of the samples started with measurements of spectral dependence of optical transmission of the substrates and AFM measurements of surface morphological characteristics. Then morphological characterization was conducted after deposition of bottom electrode and PECVD growth of p-i-n structure. After deposition of top electrode, the structure was characterized as follows:

1) Spectral measurements were conducted with a "Triax- 320" monochromator from "Jobyn Yvon" with resolution of 3.96 nm.", a "Keithley 6517A" electrometer, a thermopile sensor model 71938 from "Thermo Oriel Instruments Inc.". Xenon and halogen lamp were used for illumination.

2) AFM characterization was performed with "NEXT" from "NT-MDT". Single defects (see Fig. 4.13) found were characterized individually. For typical defect free surface morphology (see Fig. 4.13) statistical analysis of the surface was applied for the AFM images using the software "Image Analysis" (from "NT-MDT"). Surface morphology was measured for the reference substrates, plastic substrates coated by Ti deposited by DC sputtering. Ti films were employed as bottom and top electrode. p-i-n structures were deposited above plastic+Ti and surface of p-i-n structures (top n- side) before deposition of top electrode were characterized by AFM. AFM images were taken for randomly selected area segments. Dimensions of the AFM scanning were selected as S_{scan10} = 10x10 μm^2 for defect characterization and S_{scan2} = 2x2 μm^2 for typical (defect free) surface morphology.

3) Current voltage I(V) measurements: I(V) characteristics were measured with a "Keithley 6517A" electrometer in dark conditions and under constant illumination with intensity I_O= 100 mW/cm^2 (AM1.5) provided by a solar simulator "Oriel 2A".

Spectral optical transmittance T(λ) of the plastic substrates Teflon, PEN and Kapton are shown in Fig. 4.12. The short wavelengths corresponding to T=50 % and characterizing short wavelength limit are as follow: λ=280 nm for Teflon, λ=400 nm for PEN and λ=590 nm for Kapton. These data show that Teflon is a good candidate for use in solar cells as transparent substrate, because it is transparent from UV (250 nm) to NIR (900 nm) and has high transmittance T≈ 0.96 for λ>350 nm. This value is remarkably higher than those for PEN (T ≈ 0.8) and for Kapton (T≈0.76).

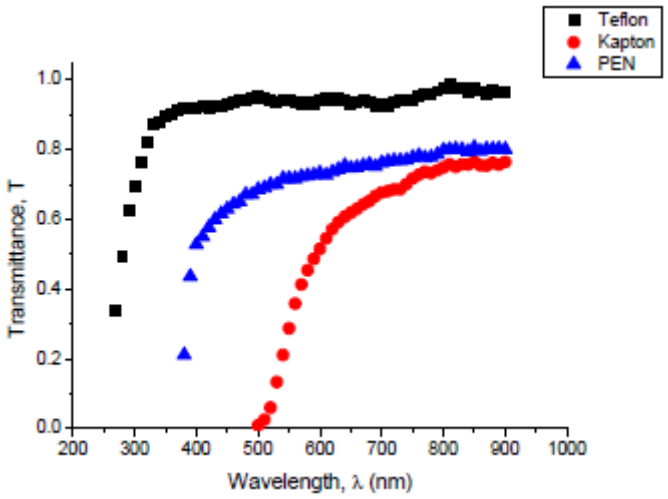

Figure 4.12. Spectral dependence of optical transmittance T(λ) of the plastic substrates.

Figure 4.13 shows AFM images of the surfaces of PEN substrate and PEN+Ti for the process No. 73. Analyzing the results of defect parameters for these two surfaces, it is observed that the maximum height S_p of defect on the surface of the PEN sample has a magnitude of S_p = 48 nm, and this value is almost the same as that on the surface of the sample 73_PEN+Ti (S_p= 47 nm). The defect width W_{def} and effective diameter of defects D_{def} have the values W= 205 nm and D= 625 nm, respectively, for the PEN substrate surface. After Ti deposition, W_{def} and D_{def} slightly reduce to W_{def}= 189 nm and D_{def}= 612 nm, respectively.

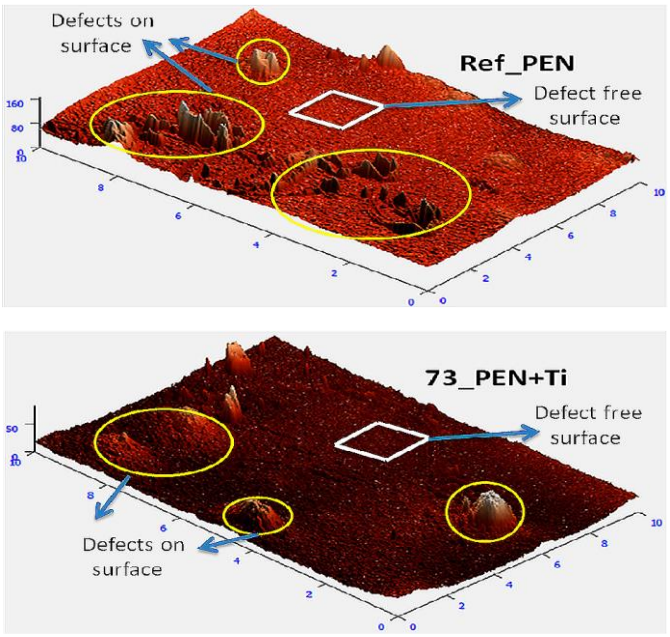

Figure 4.13. AFM images of: PEN substrate (top) and PEN+Ti metal process (bottom) for process No. 73. Defects on surfaces and defect free area are indicated.

The parameters of defects obtained for different surfaces and for the fabrication process 73 (Si:H p-i-n structure) are summarized in table 4.12. Defect parameters (maximum peak height S_p, defect width W_{def} and defect diameter D_{def}) increase their magnitudes with each consequent layer deposited. For the Kapton substrate (process No.73, sample 73_KAP), maximum peak height S_p is S_p= 36 nm, upon deposition titanium layer it increases to S_p= 66 nm (sample 73_KAP+Ti) and further increases after completing the p-i-n structure fabrication to S_p= 112 nm (sample 73_KAP+Ti+p-i-n). The defect width is W_{def}= 121 nm for Kapton substrate (sample 73_KAP), and after Ti deposition (sample 73_KAP+Ti) is W_{def}= 287 nm and after p-i-n deposition (sample 73_KAP+Ti+p-i-n) becomes W_{def}= 398 nm. The effective defect diameter for 73 KAP is D_{def}= 355 nm, for 73_KAP+Ti D_{def}= 893 nm and for 73_KAP+Ti+p-i-n D_{def}= 1101 nm. In other words, deposition Ti+p-i-n films results in "planarization" of the defects.

Maximum peak height S_p of the sample REF_PEN equals 48 nm. The defect width of REF_PEN is W_{def}= 205 nm and in 73_PEN+Ti+p-i-n, Wdef= 367 nm. Defect diameter in REF_PEN is D_{def}= 625 nm, and in 73_PEN+Ti+p-i-n, D_{def}= 1008 nm. In general defects on PEN substrate were observed "smoother" than those in Kapton substrate.

Table 4.12. AFM defect characteristics for fabrication processes No. 73 and No. 86.

Kapton polyimide					
	Process No. 73			Process No. 86	
	Ref.	Ref.+Ti	Ref.+Ti+pin	Ref.	Ref.+Ti+pin
S_p (nm)	36	66	112	36	41
W_{def} (nm)	121	287	398	121	528
D_{def} (nm)	355	893	1101	355	1258
N_{def} (defects/cm^2) x 10^6	9	8	3	9	8
PEN					
	Process No. 73			Process No. 86	
	Ref.	Ref.+Ti	Ref.+Ti+pin	Ref.	Ref.+Ti+pin
S_p (nm)	48	47	23	48	90
W_{def} (nm)	205	189	1021	205	367
D_{def} (nm)	625	612	2302	625	1008
N_{def} (defects/cm^2) x 10^6	14	6	7	14	8

Figure 4.14 shows AFM images of the typical (free of defects scanning area (arbitrarily selected) of size 2x2 μm^2) surfaces on Teflon substrate (up) and Ti+p-i-n structure (down), the latter is deposited above the titanium on Teflon. Analyzing the morphological results for the two surfaces with statistical data processing such parameters as RMS height, S_q, average grain diameter <D> and kurtosis increase after deposition p-i-n structure. The S_q changes from 7.29 nm in the reference substrate to 8.24 nm on the surface of the Ti+p-i-n device structure. The average grain diameter in the reference is <D>= 248 nm and after the p-i-n deposition is <D>= 684 nm. Kurtosis (γ_4) on the reference surface is γ_4= 2.74 and kurtosis on the surface of the p-i-n structure is γ_4= 3.13. The skewness parameter (γ_3) value suggests that the reference surface (γ_3= 0.13 > 0) changes from being dominated by peaks to that dominated by valleys onto the surface of the device (γ_3= -0.44 <0).

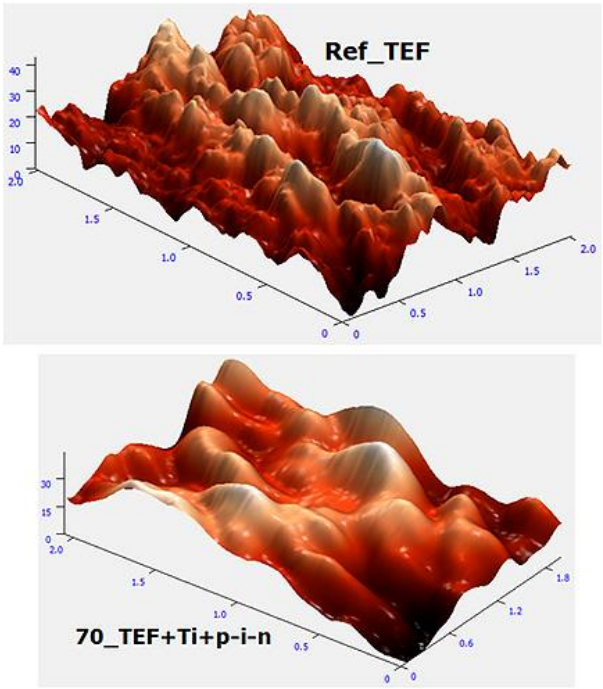

Figure 4.14. AFM images of typical area segments (defect free area, see figure 4.13): Reference Teflon substrate (up) and Ti + p-i-n structure on Teflon substrate (deposition process No. 70) (down).

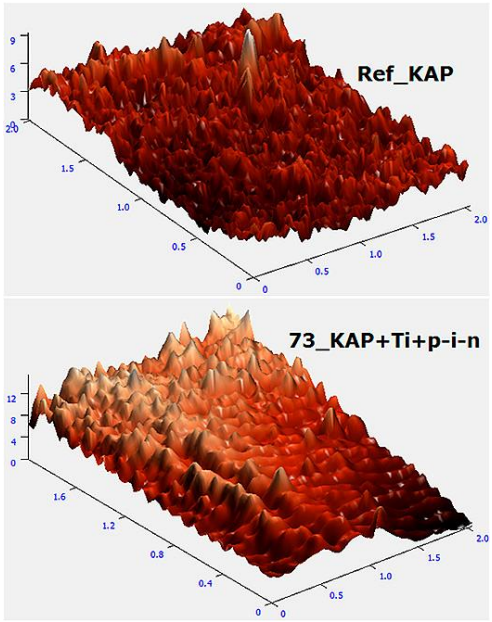

Figure 4.15. AFM images of typical area segments (without defects): Reference Kapton substrate (up) and p-i-n structure on Kapton substrate of the No. 73 process (down).

Figure 4.15 shows AFM images of the surfaces of Kapton substrate and p-i-n structure. The latter is deposited above Ti layer on Kapton. Morphological characteristics of typical surface for reference

samples and samples coated by Ti and p-i-n layers are summarized in Table 4.13. The Sq increases from Sq= 1.07 nm in the reference to Sq= 2.04 nm on the KAP-Ti p- i-n surface. The average grain diameter in the reference is <D> = 105 nm and on the KAP+Ti+p-i-n surface is <D>= 451 nm. Kurtosis on the reference surface is γ_4= 3.42 and kurtosis on the surface of the p-i-n structure is γ_4= 2.75 indicating that the peaks of the surface of the resulting p-i-n structure are less sharp than the peaks found in the reference surface. The skewness parameter value suggests that the reference surface (γ_3= -0.26) changes from being dominated by valleys to be dominated by peaks on the surface of the p-i-n structure (γ_3= 0.2).

Table 4.13. Morphology of the free of defects surfaces of the samples in fabrication process No. 86.

	Kapton polyimide		PEN		Teflon	
	Ref.	Ref.+Ti+p-i-n	Ref.	Ref.+Ti+p-i-n	Ref.	Ref.+Ti+p-i-n
$S_q\,(nm)$	1.07	2.92	1.9	7.9	7.29	35.36
$< D > (nm)$	105	923	102	825	248	1247
γ_4	3.42	3.66	2.84	2.52	2.74	2.35
γ_3	-0.26	0.32	0.11	0.36	0.13	0.63

Table 4.14. Morphology of the free of defect surfaces of the samples in fabrication process No. 73.

Kapton polyimide			
	Ref.	Ref.+Ti	Ref.+Ti+pin
S_q (nm)	1.07	6.99	2.69
<D> (nm)	105	834.5	176
γ_4 (nm)	3.42	2.55	2.75
γ_3 (nm)	-0.26	-0.15	-0.38
PEN			
	Ref.	Ref.+Ti	Ref.+Ti+pin
S_q (nm)	1.9	2.68	0.75
<D> (nm)	102	122	858
γ_4 (nm)	2.84	2.66	3.49
γ_3 (nm)	0.11	0.32	-0.36
Teflon			
	Ref.	Ref.+Ti	Ref.+Ti+pin
S_q (nm)	7.29	4.18	1.77
<D> (nm)	248	924	760
γ_4 (nm)	2.74	2.54	3.72
γ_3 (nm)	0.13	-0.2	0.73

Tables 4.13 and 4.14 presents the parameters of morphology, obtained for reference substrate surface and surface of p-i-n structures on the plastic substrate corresponding to the processes 86 and 73 for p-i-n fabrication. Positive kurtosis $\gamma_4 > 0$ is observed in all cases, indicating that the peaks are sharper than Gauss form. Sharp peaks are found in 73_TEF+Ti+p-i-n (γ_4= 3.72). Surfaces with smoother peaks are observed in the samples with p-i-n: 86_TEF+Ti+p-i-n (γ_4= 2.35), 86_PEN+Ti+p-i-n (γ_4= 2.52) and without p-i-n 73_TEF+Ti (γ_4= 2.54).

In No. 86 fabrication process, regardless of the substrate, S_q, <D> and γ_3 always increase upon deposition p-i-n structure. Thus, the changes of morphology in the samples of the No. 86 process in free defect areas suggest also “planarization” and “healing” valleys, while for the samples of the process No.73 no definitive trends were found.

Table 4.15 shows the morphological characteristics of height for the surfaces of the n-type layers of p-i-n structures deposited on different substrates. The one labeled "5C" corresponds to glass substrate and the rest correspond to plastic substrates in which the first three letters determine whether it is Kapton, PEN or Teflon.

Table 4.15 Comparison of morphological results of n-type layer height of p-i-n structures as a function of the substrate.

Interface →	5C	KAP+Ti+p-i-n	PEN+Ti+p-i-n	TEF+Ti+p-i-n
Parameter				
RMS (nm)	2.23	2.92	7.9	35.36
γ_3	0.24	0.32	0.36	0.63
γ_4	2.91	3.66	2.52	2.35

The RMS roughness value of the surface of the structure deposited on glass (RMS = 2.23 nm) is lower compared to the RMS value found on the surface of the devices deposited on the three plastic substrates used in this work. The lowest roughness observed in plastics corresponds to the structure deposited on Kapton (RMS = 2.92 nm), with a magnitude very close to that of the structure deposited on glass. A little higher there is RMS = 7.9 nm when the substrate is PEN and the rougher surface corresponds to the device manufactured on Teflon substrate (RMS = 35.36 nm).

The lowest value of skewness is due to the structure deposited on glass (γ_3 = 0.24) which means that there is only a little greater contribution of hills than valleys on that surface. With values close to the previous one, are those of structures deposited on Kapton (γ_3 = 0.32) and PEN (γ_3 = 0.36). The highest value of skewness is obtained by the structure deposited on Teflon (γ_3 = 0.63), which is interpreted as a clear greater contribution of hills than of valleys on this surface.

The value of kurtosis closest to that described by a Gaussian is that of the structure deposited on glass (γ_4 = 2.91). The kurtosis in structures deposited on plastics shows that the steepest hills correspond to the structure deposited on Kapton (γ_4 = 3.66), while for structures deposited on Teflon (γ_4 = 2.35) and PEN (γ_4 = 2.52) the form of the hills are soft.

Table 4.15 reveals that the morphological parameters change considerably in multilayer structures when there are different substrates. Finally, the performance characteristic of the structures were measured for general diagnostic.

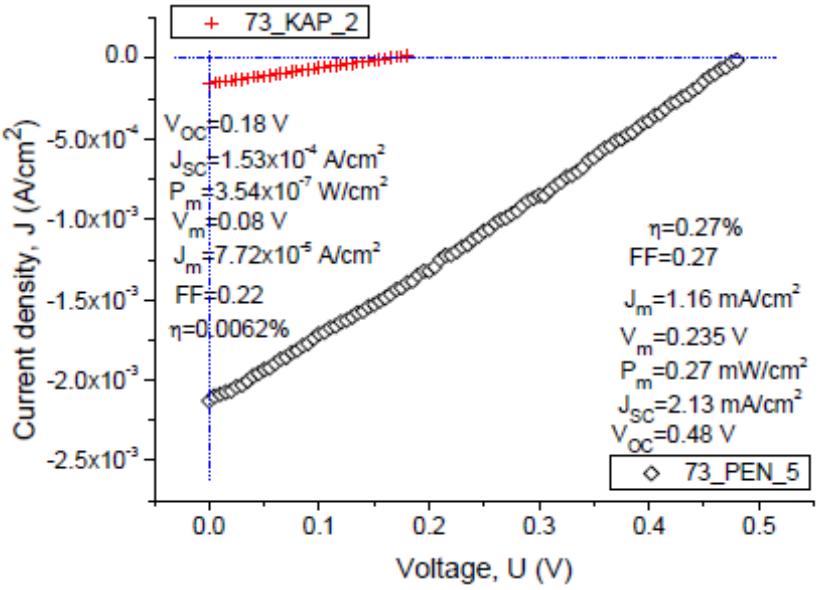

Figure 4.16. Solar cell output parameters for two pin structures with PEN and Kapton substrate.

Figure 4.16 shows two density current-voltage J(V) curves under illumination condition used to determine the performance characteristics of p-i-n solar cells deposited on the Kapton and PEN substrates for process No.73. p-i-n Structures fabricated in process No.73 on Teflon did not allow electrical characterization because of problems of adherence and pin shots. These J(V) curves show that output current and voltage are controlled by low value shunt resistor. The open circuit voltage for structure on Kapton substrate is V_{oc}= 0.18 V and for the device on PEN substrate is V_{oc}= 0.48 V. The short circuit current density of the sample 73_PEN_5 (J_{sc}= 2.13x10^{-3} A/cm^2) is larger than that of the sample 73_KAP_2 (J_{sc}= 1.53x10^{-4} A/cm^2). Higher values of both V_{oc} and J_{sc} for solar cell on PEN substrate (73_PEN_5) result in a higher power output Pm= 0.27 mW/cm^2.

4.2 Study of argon plasma treatment to enhance polymer and contact adhesion on flexible substrates.

Initially, the Teflon substrates were cleaned with Isopropanol for 30 seconds, shaking the samples continuously and then drying them in laminar flow. The original adherence of photoresist to plastic substrates is poor. In Figure 4.17 it is shown a failure deposition of photoresist on Teflon substrates.

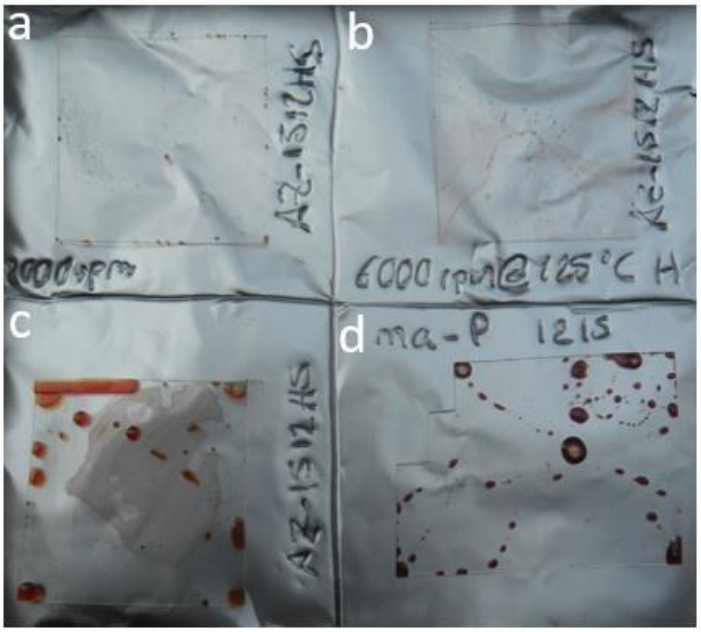

Figure 4.17. Teflon samples without Ar plasma treatment to which photoresist was deposited without success.

In figure 4.17.b photoresist AZ 1512 HS is deposited at 6000 rpm and it was no satisfactory result, then with the same photoresist, the speed was reduced to 2000 rpm (figure 4.17.a) and no adherence was obtained. Observing the above, the revolutions are reduced to 500 rpm (figure 4.17.c) and there was no adhesion. Finally, it was tried deposition at 500 rpm with the photoresist ma-P 1215 (figure 4.17.d) obtaining the same result as was obtained with the AZ 1512 HS photoresist.

To enhance adhesion to the plastic substrate was optimize and propose the follow Ar treatment conditions: Preheating was carried out for 5 minutes and the plasma processing was done in the PL2 chamber of the PECVD MVSystem, Power 30 W. – Pressure 0.3 Torr. – Time 6 minutes. - Temperature: 110°C and room temperature (RT).

Figure 4.18 in its left column shows the Teflon substrates that were subjected to Argon plasma treatment at room temperature. The film deposited was photoresist ma-P 1215 and the revolutions used in this stage were 1000, 2000, 3000 and 4000 rpm. At 1000 rpm "dirt" is seen because the sample size was smaller than that of the spinner holder, the remaining samples are larger and clean and a good deposit of film is noted on them. Figure 4.18 in its right column shows the Teflon substrates that were subjected to Argon plasma treatment at a temperature of 110 ° C. The film deposited was photoresist ma-P 1215 and the revolutions used in this stage were 400, 500, 1000 and 3000 rpm. As the revolutions increase, it is possible to observe thinner and more uniform films.

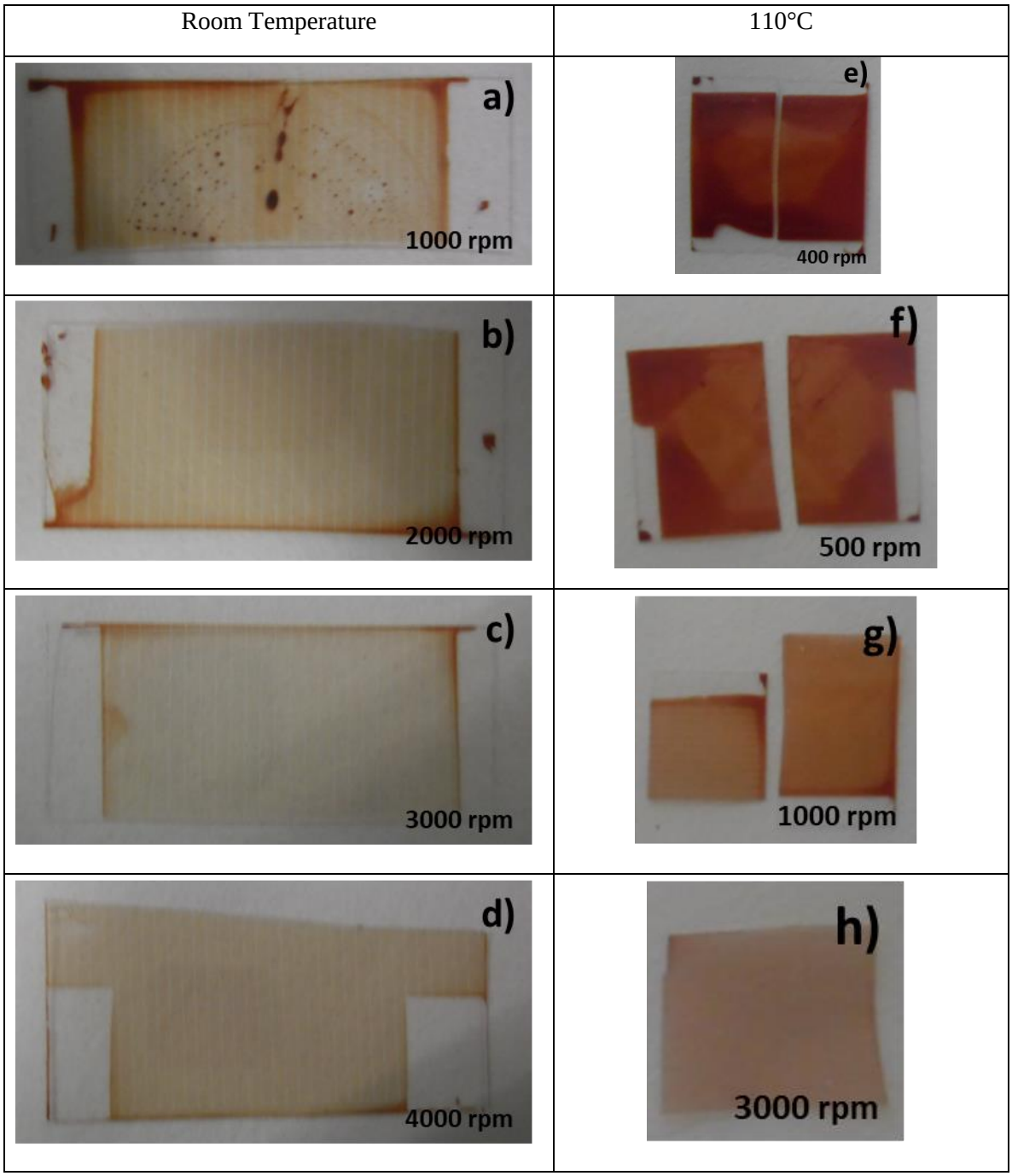

Figure 4.18. Photoresist ma-P 1215 deposited at different revolutions on Teflon substrate treated with Ar plasma at RT and 110 ° C.

Figure 4.19 in its left column shows the Teflon substrates that were subjected to Ar plasma treatment at temperature 110 ° C. The film deposited was photoresist AZ 1512 HS and the revolutions used in this stage were 3000, 4000 and 5000 rpm. The photographs show a uniform deposit and decrease in transmittance. Figure 4.19 in its right column shows the

Teflon substrates that were subjected to Ar plasma treatment at temperature 110 ° C. The film deposited was photoresist AZ 2020 and the revolutions used in this stage were 3000, 4000 and 5000 rpm. The photoresist AZ 2020 is used because it is transparent or semitransparent, and because it is not easily removed.

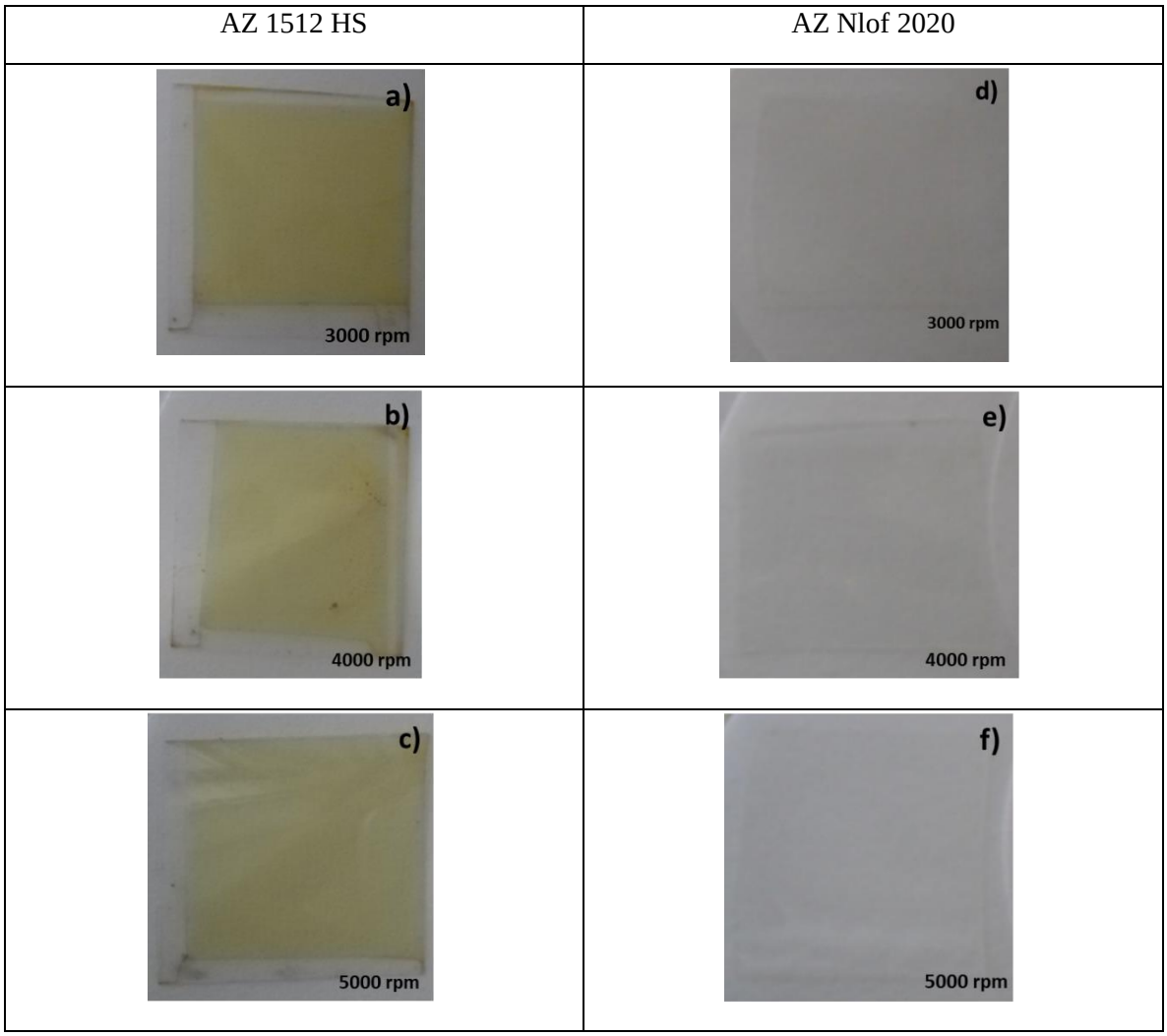

Figure 4.19. Photoresist AZ 1512 HS and AZ 2020 deposited on Teflon substrate at different revolutions.

Figure 4.20 shows the transmittance curves of PEN and Teflon substrates as well as different photoresist films deposited on Teflon substrates. On the left are positive photoresist systems on Teflon which cause the passage of photons to be lost at low wavelengths, although for most of the visible spectrum this system has higher transmittance than the reference PEN substrate. The 340-470 nm region has a different spectral characteristic as a function of the thickness of the positive photoresist.

On the right are the curves for negative photoresist deposited on Teflon at different rpm. With negative photoresist there is greater uniformity in the spectral response compared to positive photoresist.

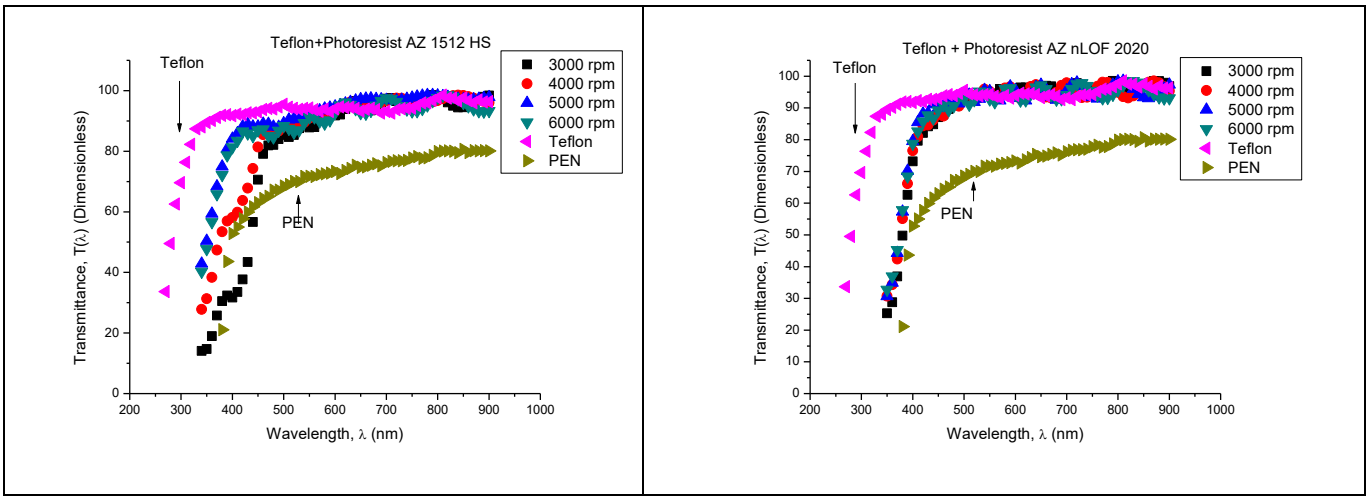

Figure 4.20. Transmittance systems Teflon + Photoresist in function of rpm. (Left) Positive Photoresist. (Right) Photoresist negative.

With the negative photoresist, the spectrum is used a little more in relation to the positive one, observing the curves near 400 nm it is possible to declare that all the samples with negative photoresist obtained higher transmittance than the reference PEN substrate. The transmittance of the surface modification layer / Teflon system is better than that of the PEN and Kapton substrates.

4.3 Study of planarization of defects on flexible substrates.

The objective of this section is to obtain films as frontal contact with low resistance and high transmittance via defects planarization in plastic substrates, to be used in flexible photovoltaic structures.

4.3.1 Planarization via AZO thickness

AZO electrodes with different thickness and frontal configuration on plastic substrates (PEN, Kapton polyimide and Teflon) were used to study planarization of morphology. Four (4) different thicknesses were available: 100 Å, 260 Å, 1500 Å and 2300 Å (figure 4.21).

Figure 4.21. AZO systems of different thicknesses deposited on plastics.

In table 4.16 the morphological characteristics of AZO films of thickness 100 Å deposited on plastic substrates are shown.

Table 4.16. Results of AZO film morphology 100 Å thick deposited on plastic substrates.

AZO 100			
	Teflon	PEN	Kapton
RMS roughness (nm)	9.7	0.37	1.11
Average height (nm)	23.1	1.74	4.49
Surface Skewness	-0.42	-0.02	0.02
Surface kurtosis	2.15	3.04	3.11

In table 4.16 the RMS roughness of AZO_100 / Teflon is the highest with a value of 9.7 nm, AZO_100 / Kapton has RMS = 1.11 nm and AZO_100 / PEN has the lowest RMS roughness = 0.37 nm.

The average height of AZO_100 / Teflon is the highest with a value of 23.1 nm, AZO_100 / Kapton has <H> = 4.49 nm and AZO_100 / PEN has the lowest average height <H> = 1.74 nm.

The skewness parameter (γ_3) takes values very close to 0 in the samples AZO_100 / PEN and AZO_100 / Kapton, $\gamma_3 = -0.02$ and $\gamma_3 = 0.02$ respectively. The sample AZO_100 / Teflon has a negative γ_3 with magnitude -0.42.

The kurtosis parameter (γ_4) takes values very close to 3 in the samples AZO_100 / PEN and AZO_100 / Kapton, $\gamma_4 = 3.04$ and $\gamma_3 = 3.11$ respectively. The sample AZO_100 / Teflon has a γ_4 less than 3, this being $\gamma_4 = 2.15$.

In table 4.17 the morphological characteristics of AZO films of thickness 260 Å deposited on plastic substrates are shown.

Table 4.17. Results of AZO film morphology 260 Å thick deposited on plastic substrates.

AZO 260			
	Teflon	PEN	Kapton
RMS roughness (nm)	7.99	1.67	3.07
Average height (nm)	26.82	6.22	10.55
Surface Skewness	-0.09	0.17	0.35
Surface kurtosis	2.70	3.18	3.89

In table 4.17 the RMS roughness of AZO_260 / Teflon is the highest with a value of 7.99 nm, AZO_260 / Kapton has RMS = 3.07 nm and AZO_260 / PEN has the lowest roughness RMS = 1.67 nm.

The average height of AZO_260 / Teflon is the highest with a value of 26.82 nm, AZO_260 / Kapton has <H> = 10.55 nm and AZO_260 / PEN has the lowest average height <H> = 6.22 nm.

The skewness parameter (γ_3) takes values very close to 0 in the sample AZO_260 / Teflon. The samples AZO_260 / PEN and AZO_260 / Kapton have values of γ_3 positive being γ_3 = 0.17 and γ_3 = 0.35 respectively.

The sample AZO_260 / Kapton has a value γ_4 = 3.89, which is the largest of the three samples. The lowest kurtosis is exhibited by the sample AZO_260 / Teflon with γ_4 = 2.70 and at an intermediate level AZO_260 / PEN has γ_4 = 3.18.

In table 4.18 the morphological characteristics of AZO films of 1500 Å thickness deposited on plastic substrates are shown.

Table 4.18. Results of AZO film morphology 1500 Å thick deposited on plastic substrates.

AZO 1500			
	Teflon	PEN	Kapton
RMS roughness (nm)	9.0	1.39	1.85
Average height (nm)	25.98	5.83	8.69
Surface Skewness	0.45	0.15	0.37
Surface kurtosis	3.10	3.15	4.8

In table 4.18 the RMS roughness of AZO_1500 / Teflon is the highest with a value of 9.0 nm, AZO_1500 / Kapton has RMS = 1.85 nm and AZO_1500 / PEN has the lowest roughness RMS = 1.39 nm.

The average height of AZO_1500 / Teflon is the highest with a value of 25.98 nm, AZO_1500 / Kapton has <H> = 8.69 nm and AZO_1500 / PEN has the lowest average height <H> = 5.83 nm.

The samples AZO_1500 / Teflon and AZO_1500 / Kapton have values very close to each other of γ_3, namely, 0.45 and 0.37 respectively. AZO_1500 / PEN exhibits γ_3 = 0.15.

The samples AZO_1500 / Teflon and AZO_1500 / PEN have very close values of γ_4, 3.10 and 3.15 respectively. AZO_1500 / Kapton shows γ_4 = 4.8.

In table 4.19 the morphological characteristics of AZO films of 2300 Å thickness deposited on plastic substrates are shown.

Table 4.19. Results of AZO film morphology 2300 Å thick deposited on plastic substrates.

AZO 2300			
	Teflon	PEN	Kapton
RMS roughness (nm)	6.98	1.00	1.41
Average height (nm)	21.61	3.29	3.63
Surface Skewness	-0.18	-0.21	3.02
Surface kurtosis	2.76	2.01	17.63

In table 4.19 the RMS roughness of AZO_2300 / Teflon is the highest with a value of 6.98 nm. AZO_2300 / PEN and AZO_2300 / Kapton present rugosities close in magnitude, RMS = 1.00 and RMS = 1.41 respectively.

The average height of AZO_2300 / Teflon is the highest with a value of 21.61 nm. AZO_2300 / PEN and AZO_2300 / Kapton have <H> close in magnitude, <H> = 3.29 and <H> = 3.63 respectively.

AZO_2300 / Teflon and AZO_2300 / PEN possess γ_3 of similar magnitude, $\gamma\_3 = -0.18$ and $\gamma\_3 = -0.21$ respectively, and these values are negative and close to 0. AZO_2300 / Kapton exhibits a higher γ_3 with magnitude 3.02.

AZO_2300 / Teflon and AZO_2300 / PEN possess γ_4 of similar magnitude, $\gamma_4 = 2.76$ and $\gamma_4 = 2.01$ respectively. AZO_2300 / Kapton exhibits a higher γ_4 with magnitude 17.63.

4.3.2 Planarization via AZO/Carbon layers

AZO/Carbon electrodes with frontal configuration on plastic substrates (PEN, Kapton polyimide and Teflón) were used to study planarization of morphology (figure 4.21).

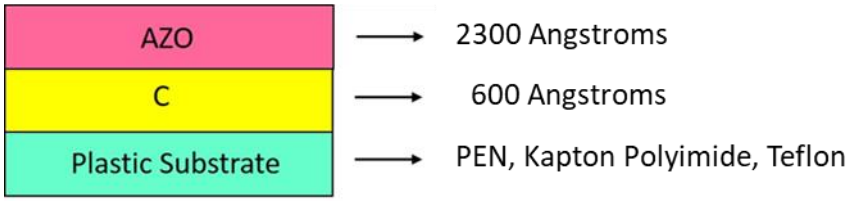

Figure 4.22. AZO / C system deposited on plastics.

In table 4.20 the morphological characteristics of AZO / C films deposited on plastic substrates are shown.

Table 4.20. Morphology results of C + AZO deposited on plastic substrates.

C + AZO			
	Teflon	PEN	Kapton
RMS roughness (nm)	7.34	3.63	0.87
Average height (nm)	20.77	8.32	2.87
Surface Skewness	0.02	1.07	0.42
Surface kurtosis	2.77	4.66	3.28

In Table 4.20 the roughness of AZO / C / Teflon is the highest with magnitude RMS = 7.34 nm. The lowest roughness corresponds to AZO / C / Kapton with RMS = 0.87 nm and AZO / C / PEN has RMS = 3.63 nm.

The average height of AZO / C / Teflon is the highest with magnitude <H> = 20.77 nm. The lowest roughness corresponds to AZO / C / Kapton with <H> = 2.87 nm and AZO / C / PEN has <H> = 8.32 nm.

AZO / C / Teflon has $\gamma_3 = 0.02$, at an intermediate level it is AZO / C / Kapton with $\gamma_3 = 0.42$ and with the highest value of skewness AZO / C / PEN with $\gamma_3 = 1.07$.

AZO / C / Teflon exhibits kurtosis less than 3, namely, $\gamma_4 = 2.77$. AZO / C / PEN and AZO / C / Kapton have positive γ_4 values, being the closest to 3 that of AZO / C / Kapton ($\gamma_4 = 3.28$) and with a higher value we have AZO / C / PEN ($\gamma_4 = 4.66$).

4.3.3 Planarization via AZO/SiC:H layers

AZO/SiC electrodes with frontal configuration on plastic substrates (PEN, Kapton polyimide and Teflón) were used to study planarization of morphology (figure 4.21).

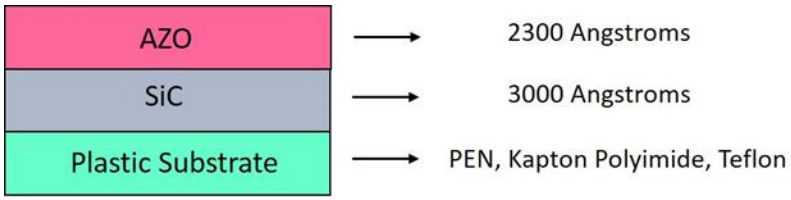

Figure 4.23. AZO / SiC system deposited on plastics.

In table 4.21 the morphological characteristics of AZO / SiC films deposited on plastic substrates are shown.

Table 4.21. Morphology results of SiC + AZO deposited on plastic substrates.

SiC + AZO			
	Teflon	PEN	Kapton
RMS roughness (nm)	4.28	4.14	5.35
Average height (nm)	11.66	13.48	13.04
Surface Skewness	0.68	0.29	2.3
Surface kurtosis	4.01	3.13	11.67

In Table 4.21 the samples AZO / SiC / Teflon and AZO / SiC / PEN have roughness values close to each other, RMS = 4.28 nm and RMS = 4.14nm respectively. With a slightly higher value we have the sample AZO / SiC / Kapton with RMS = 5.35 nm.

the samples AZO / SiC / PEN and AZO / SiC / Kapton have height values close to each other, <H> = 13.48 nm and <H> = 13.04 nm respectively. With a slightly lower value, the AZO / SiC / Teflon sample is <H> = 11.66 nm.

All samples have positive values of γ_3, with close values between samples AZO / SiC / Teflon and AZO / SiC / PEN, $\gamma_3 = 0.68$ and $\gamma_3 = 0.29$ respectively. AZO / SiC / Kapton has γ_3 greater with γ_3 = 2.3.

AZO / SiC / Kapton exhibits a very high value of γ_4, with a magnitude of 11.67, while AZO / SiC / Teflon and AZO / SiC / PEN exhibit values closer to 3, namely, $\gamma_4 = 4.01$ and $\gamma_4 = 3.13$ respectively.

Figure 4.24 shows a "graphic" summary of the main morphological characteristics of the different frontal electrode systems studied.

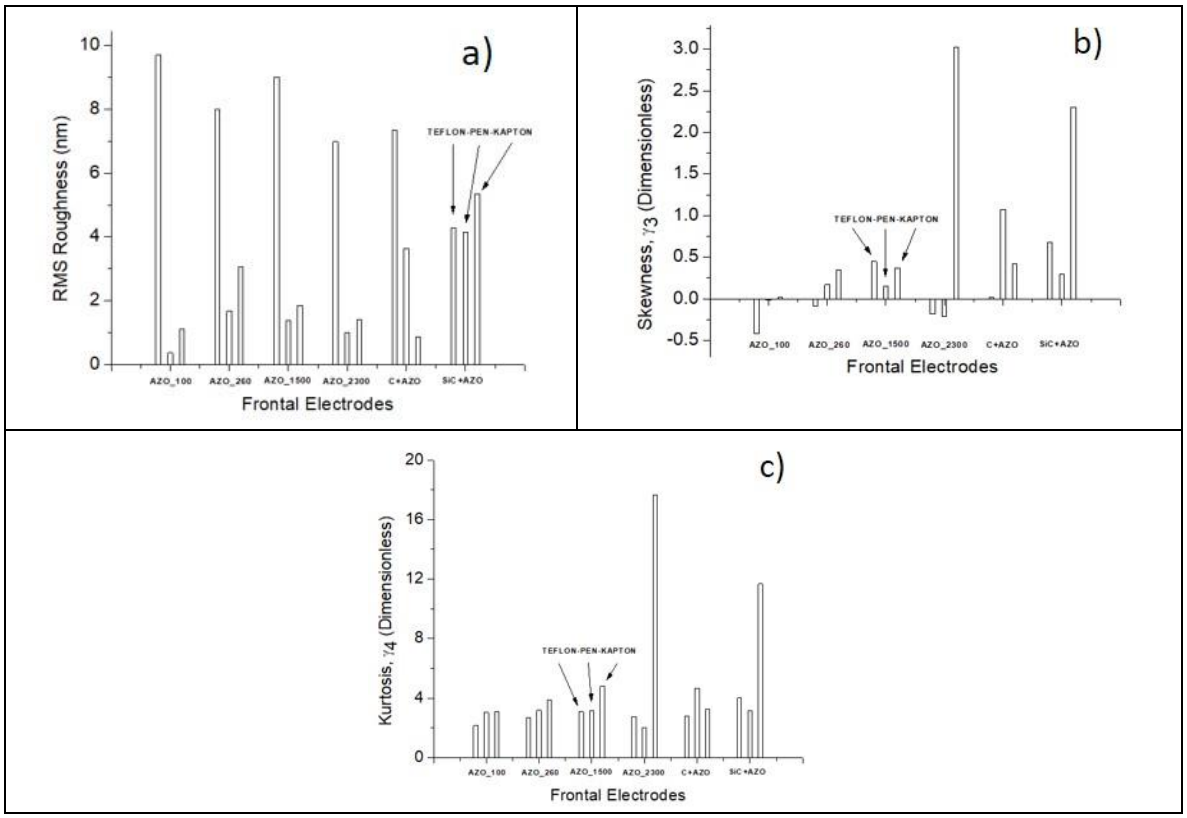

Figure 4.24. Summary of morphological characteristics of frontal electrodes.

Figure 4.24.a shows the roughness summary of the different frontal electrodes. The x axis consists of 6 different electrode systems and each in turn consists of three substrates, que vistos de izquierda a derecha siempre serán Teflon, PEN y Kapton. Figure 4.24 b shows the summary of the skewness parameter and c) the kurtosis summary of the different frontal electrodes.

SiC + AZO electrodes exhibit greater uniformity of roughness. The roughness of electrodes (AZO 150 nm, AZO 230 nm and C + AZO) deposited on Teflon is greater than the roughness of the same electrodes deposited on PEN and Kapton.

AZO 150 nm electrodes exhibit greater uniformity of the γ_3 parameter. Electrodes AZO 230 nm show values of γ_3 very high when the substrate is Kapton and negative values on Teflon and PEN.

Electrodes deposited on Kapton tend to have very high γ_4 values. In electrodes deposited on Teflon, values of γ_4 very close to 3 are observed depending on the substrate, the electrodes with more uniformity of γ_4 are those of AZO 150 nm and C + AZO.

Results of transmittance measurements of the different frontal electrode systems in the p-i-n configuration studied in the previous section, are shown in Figure 4.25 for each plastic substrate used.

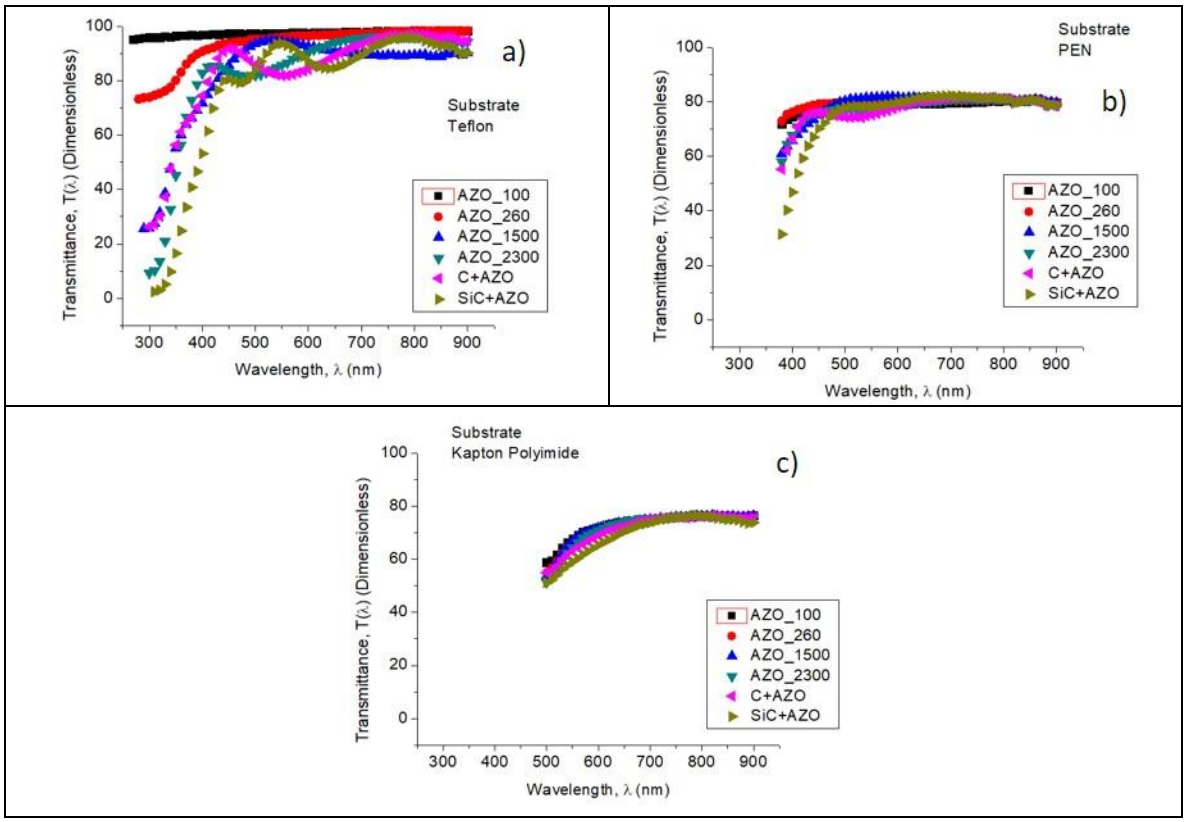

Figure 4.25. Transmission results of different frontal electrodes.

Figure 4.25.a shows the transmittance results of the different frontal electrodes deposited on Teflon substrate. To compare them, the average transmittance in the range 400-850 nm has been determined. The AZO_100 sample has an average transmittance equal to 97.74%. The sample AZO_260 has T_prom (Vis) = 96.36%. The sample AZO_1500 has T_prom (Vis) = 89.42%. An average transmittance of 90.28% corresponds to AZO_2300. The C + AZO system showed T_prom (Vis) = 89.52% and finally SiC + AZO has T_prom (Vis) = 87.07%.

Figure 4.25.b shows the transmittance results of electrodes deposited on PEN substrate. The AZO_100 sample has an average transmittance equal to 78.81%. The sample AZO_260 has T_prom (Vis) = 80.04%. The sample AZO_1500 has T_prom (Vis) = 79.40%. An average transmittance of 77.89% corresponds to AZO_2300. The C + AZO system showed T_prom (Vis) = 76.95% and finally SiC + AZO has T_prom (Vis) = 75.63%.

Figure 4.25.c shows the transmittance results of electrodes deposited on Kapton substrate. The AZO_100 sample has an average transmittance equal to 72.52%. The sample AZO_260 has T_prom (Vis) = 71.84%. The sample AZO_1500 has T_prom (Vis) = 71.95%. An average transmittance of 72.07% corresponds to AZO_2300. The C + AZO system showed T_prom (Vis) = 71.50% and finally SiC + AZO has T_prom (Vis) = 70.67%.

4.3.4 Planarization via photoresist layer

Photoresist (PR) layer deposited on plastic substrates (PEN, Kapton polyimide and Teflón) was used to study planarization of morphology (figure 4.26).

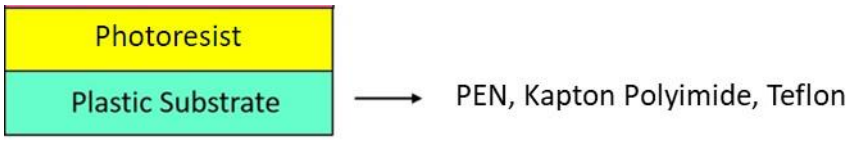

Figure 4.26. Planarization of plastic substrates by means of photoresist layer.

In table 4.22 the morphological characteristics of photoresist films deposited on plastic substrates are shown.

Table 4.22. Morphology results of photoresist nlof 2020 deposited on plastic substrates.

Photoresist			
	Teflon	PEN	Kapton
RMS roughness (nm)	0.20	4.52	1.77
Average height (nm)	0.85	12.59	8.98
Surface Skewness	0.09	0.88	0.03
Surface kurtosis	3.00	5.18	3.47

In table 4.22 the PR / PEN roughness is the highest with magnitude 4.52 nm. PR / Teflon exhibits a very low RMS roughness = 0.20 nm and an intermediate value between the analyzed samples has PR / Kapton with RMS = 1.77 nm.

The observed trend for the RMS parameter is the same as the average height. From highest to lowest <H> we have: PR / PEN (<H> = 12.59 nm), PR / Kapton (<H> = 8.98 nm) and PR / Teflon (<H> = 0.85 nm).

PR / Teflon and PR / Kapton have γ_3 of positive magnitude and close to 0. PR / PEN also has positive γ_3 but with greater magnitude, namely, $\gamma_3 = 0.88$.

PR / Teflon and PR / Kapton have γ_4 with magnitude close to 3, $\gamma_4 = 3.00$ and $\gamma_4 = 3.47$ respectively. PR / PEN possesses γ_4 = 5.18, which is the highest kurtosis.

Figure 4.27 shows the results of the transmittance measurements of photoresist films deposited on the plastic substrates.

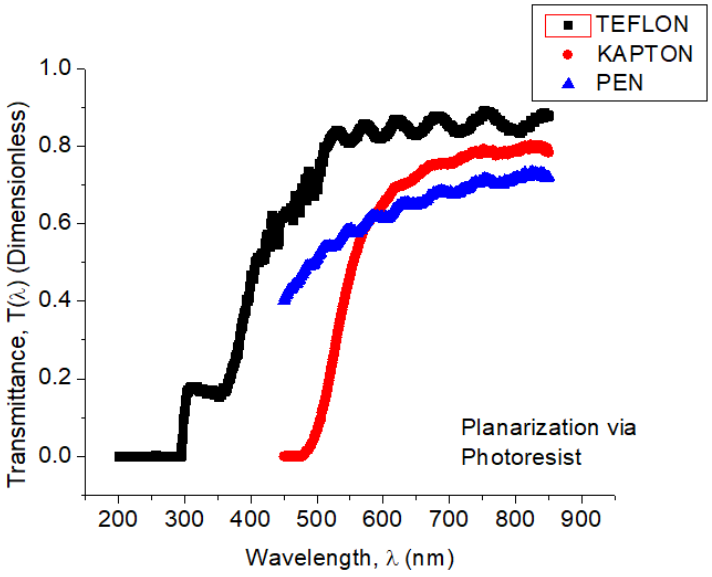

Figure 4.27 Results of transmittance photoresist films deposited on plastics.

The PR / Teflon sample has an average transmittance in the range of wavelengths 400-850 nm equal to 79.30%. PR / Kapton has T_prom (Vis) = 63.03% and PR / PEN exhibited T_prom (Vis) = 58.00%.

4.3.5 Planarization via Carbon layer

Carbon layer deposited on plastic substrates (PEN, Kapton polyimide and Teflón) was used to study planarization of morphology (figure 4.28).

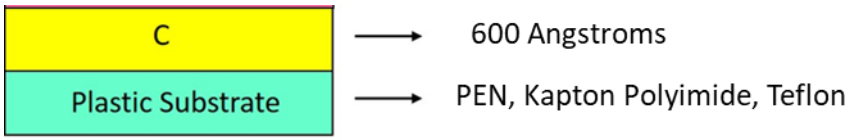

Figure 4.28. Planarization of plastic substrates by means of a carbon layer.

In table 4.23 the morphological characteristics of carbon films deposited on plastic substrates are shown.

Table 4.23 Morphology results of carbon layer deposited on plastic substrates.

Carbon			
	Teflon	PEN	Kapton
RMS roughness (nm)	4.77	1.95	4.79
Average height (nm)	15.61	6.06	19.92
Surface Skewness	0.22	0.53	0.20
Surface kurtosis	3.29	3.79	3.61

In table 4.23 C / Teflon and C / Kapton have similar RMS value, that is, RMS = 4.77 nm and RMS = 4.79 nm respectively. C / PEN has lower roughness (RMS = 1.95 nm).

C / Kapton exhibits the highest value of <H> with magnitude <H> = 19.92 nm. The smaller <H> corresponds to C / PEN (<H> = 6.06 nm) and C / Teflon shows <H> = 15.61 nm.

C / Teflon and C / Kapton have a similar value of γ_3, 0.22 and 0.20 respectively. C / PEN has a greater γ_3 with a magnitude equal to 0.53.

C / Teflon, C / PEN and C / Kapton have similar values of γ_4, 3.29, 3.79 and 3.61 respectively.

Figure 4.29 shows the results of the transmittance measurements of carbon films deposited on the plastic substrates.

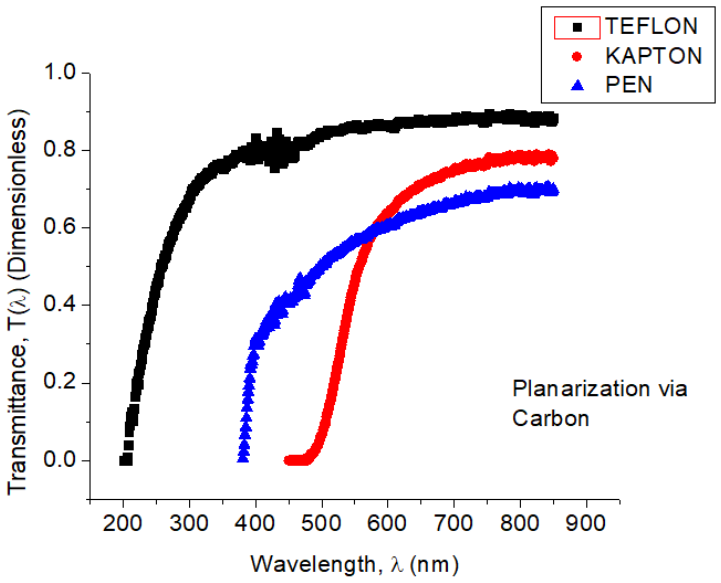

Figure 4.29 Transmission results carbon films deposited on plastics.

The sample C / Teflon has an average transmittance in the range of wavelengths 400-850 nm equal to 85.87%. PR / Kapton has T_prom (Vis) = 57.00% and PR / PEN exhibited T_prom (Vis) = 59.00%.

4.4 Fabrication and results of flexible solar cells

4.4.1 Effect of photoresist on current density-voltage results under AM1.5 illumination

Figure 4.30 shows the schematics of two pin structures fabricated on PEN substrate. These structures differ in that a photoresist layer has been incorporated between the bottom electrode and the substrate in order to investigate its effect on performance characteristics.

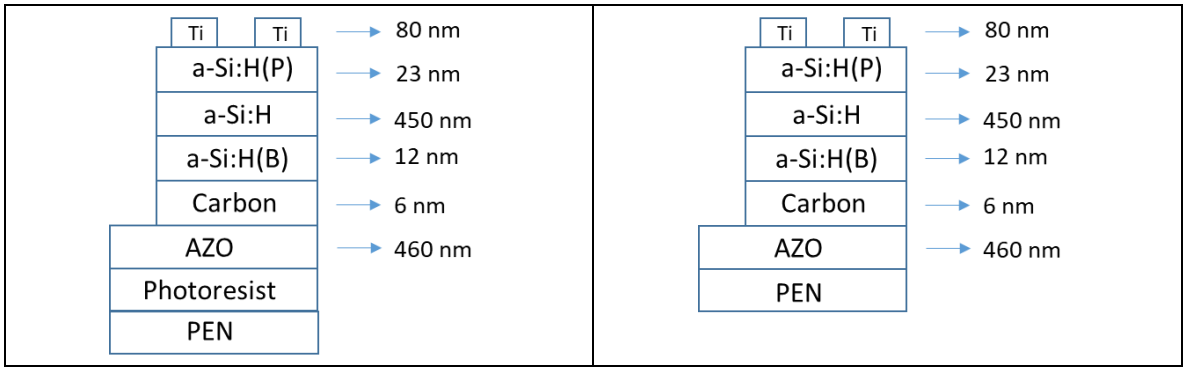

Figure 4.30. Esquemáticos de estructuras pin depositadas sobre PEN.

The p-i-n structures in Figure 4.30 have a TCO AZO of 460 nm thickness, a thin layer of carbon that was manufactured for 60 seconds and a layer of a-Si: H (B) of 12 nm thickness. The intrinsic a-Si:H film has a thickness of 450 nm, the n-type a-Si: H film is 23 nm thick and the top electrode is made of Ti material.

Table 4.24 corresponds to the fabrication conditions of the structures shown in Figure 4.30.

Table 4.24. Deposition conditions of structures p-i-n of the process 354.

Operation	Chamber	Deposition parameters				
		Pressure (Torr)	Power W	Temperature. (°C) Display/Substrate	Time (s)	Flow (sccm)
AZO layer	PL3	0.3	100	193/150	5400	12 (Ar)
Plasma processing	PL2	0.002	30	265/160	300	12 (Ar)
Carbon layer	PL2	0.69	3	265/160	60	4.5 (CH_4)
p-type layer	PL2	0.69	3	265/160	90+30	30 (SiH_4), 3 (B_2H_6), 7 (CH_4)
Intrinsic layer	PL4	0.55	3	265/160	4500	10 (SiH_4)
n-type layer	PL7	0.55	3	265/160	230	30 (SiH_4), 0.3 (PH_3)

Table 4.24 shows that the deposition temperature used is 160 ° C, with the exception of the AZO film, which was deposited at 150 ° C. It should be mentioned that the fabrication process 354 makes use of Ar plasma treatment to improve the surface characteristics of the

plastic substrate, mainly the adhesion. The pressure used for the carbon buffer layer and the p-type a-Si:H film is 0.69 Torr and the pressure for the intrinsic and n-type films is 0.55 Torr. The AZO film is deposited by the sputtering technique and such a system is part of the RF PECVD MVS system. The power was adjusted to 3 W during the deposition of the carbon films and those of p-, n- and intrinsic a-Si:H films.

Figure 4.31 is a comparison of performance characteristics of process 354 with process 73.

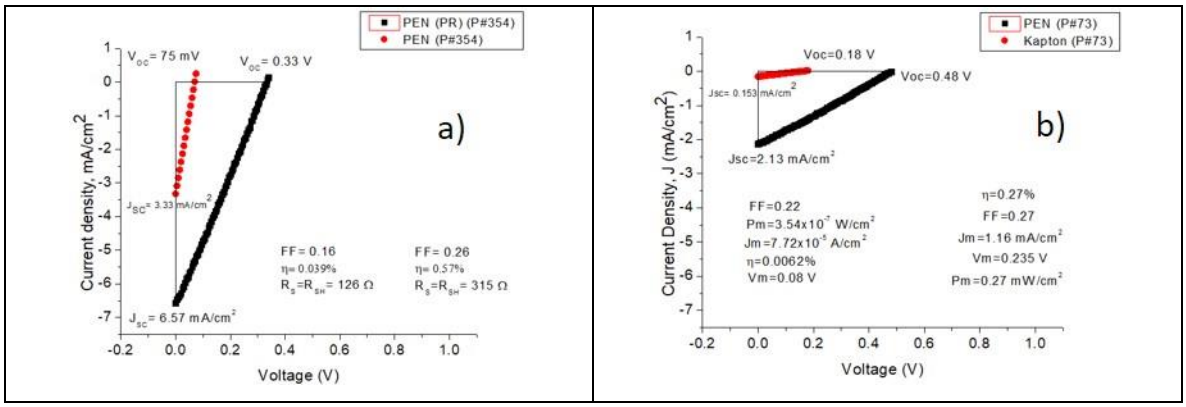

Figure 4.31. Performance characteristics of p-i-n structures deposited on flexible substrates corresponding to processes 354 and 73.

The process 73 was the first to be characterized by means of J-V measurements. The process 73 did not have treatment with Ar plasma nor a layer of planarization on the plastic substrate. Substrates PEN and Kapton were used in the process 73, the device deposited on Kapton obtained an efficiency of 0.0062% and an FF = 0.22. The Voc value was equal to 0.18 V and that of the current density was 0.153 mA / cm^2. The structure deposited on PEN achieved better electrical results than the previous one, obviously because the PEN substrate is more transparent than Kapton. The efficiency was 0.27% and FF = 0.27. The Voc value reached 0.48 V and Jsc was 2.13 mA / cm^2. Comparing the structure of the process 73 with that shown in Figure 4.31.a, it is possible to declare that there has been an improvement in the short circuit current density. The 354 process consists of two samples, one with photoresist (PR) layer and one without it. The device without PR has efficiency of 0.039% and a small value of FF equal to 0.16. It also presents low Voc, with magnitude 75 mV and Jsc = 3.33 mA / cm2. The structure with PR layer achieved an efficiency of 0.57% although a poor FF of 0.26. Its Voc = 0.33V and its Jsc = 6.57 mA / cm^2.

Next, a comparison of performance characteristics will be made for the structure of the process 73 deposited on PEN and the structure of the process 354 that includes the photoresist film.

The open circuit voltage decreased by 31.25% going from process 73 to 354. The short circuit current density increased by 3.08 times, the fill factor is almost the same in both stages and the efficiency increased 2.11 times.

4.4.2 p-i-n structure deposited on PEN without a planarization layer.

The schematic diagram of the pin structure fabricated in process 343 is shown in Figure 4.32.

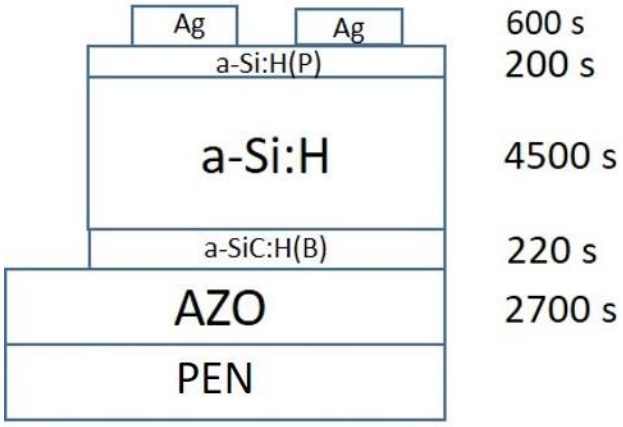

Figure 4.32. Schematic of pin structure deposited on PEN of process 343.

In the figure 4.32 the times used to manufacture each layer that makes up the device are observed. Two thousand seven hundred seconds of deposit of AZO correspond to a thickness of 230 nm. The thickness of the intrinsic layer remained the same for almost all the deposits in the doctoral work. The material of the top electrode is Ag. The layers type p and n respectively have thicknesses of 22 and 20 nm.

Table 4.25 presents the deposition conditions of the structure seen in Figure 4.32.

Table 4.25. Fabrication conditions of structure p-i-n of the process 343.

Operation	Chamber	Deposition parameters			
		Pressure (Torr)	Power W	Time (s)	Flow (sccm)
Plasma processing	PL2	0.3	30	300	12 (Ar)
Bottom electrode	AZO	0.002	100	2700	12 (Ar)
Carbon layer	PL2	0.69	3	60	4.5 (CH_4)
p-type layer	PL2	0.69	3	220 (*)	30 (SiH_4), 3 (B_2H_6), 12 (CH_4)
Intrinsic layer	PL4	0.55	3	4500	10 (SiH_4)
n-layer)	PL7	0.55	3	200	30 (SiH_4), 0.3 (PH_3)
Top electrode	Ag	0.002	75	600	10 (Ar)

In table 4.25 it is possible to appreciate the gas flows that were used during the deposition. To deposit p-type layer, 30 sccm of SiH_4, 3 sccm of diborane and 12 sccm of methane were used. The n-type layer was formed with 30 sccm of SiH_4 and 0.3 sccm of phosphine. The intrinsic layer used a continuous flow of 10 sccm of SiH_4. AZO and Ag electrodes were deposited by sputtering. The pressures used to manufacture the stack of layers from the

carbon buffer layer to the n-type a-Si:H film retain the same values as those in the deposition of 354 process.

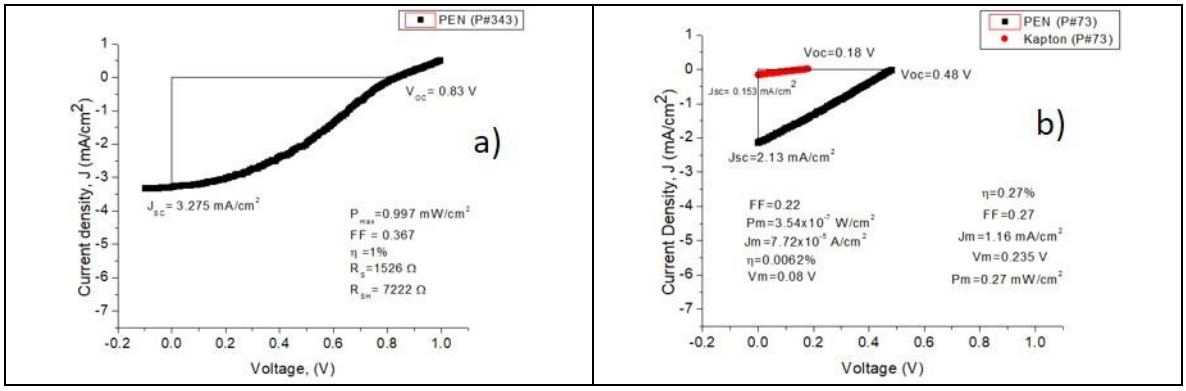

Figure 4.33. Performance characteristics of p-i-n structures deposited on flexible substrates corresponding to processes 343 and 73.

Figure 4.33.a shows the performance characteristics of a p-i-n photovoltaic device deposited on PEN. The open circuit voltage reached a value of 0.83 V and a short circuit current density of 3.28 mA / cm^2. Its efficiency was 1% and FF = 0.37. A visual inspection shows that the shape of the curve is no longer a straight line, for this reason there is a series resistance value different from that of shunt resistance, namely 1.5 kΩ and 7.2 kΩ respectively.

A comparison of performance characteristics for the structure of the process 73 and the structure of the process 343 will be made below.

Open circuit voltage increased 1.73 times between process 73 and 343. The short circuit current density increased by 1.54 times, the fill factor increased 1.37 times and the efficiency increased 3.7 times.

4.4.3 AZO/PEDOT:PSS interfaces in hybrid solar cell on flexible substrates

Organic materials based on polymer semiconductors have been in focus during the last decade. The most studied materials such as the bulk heterojunction P3HT:PCBM and the conductive semiconductor PEDOT:PSS have been widely implemented in new organic thin-film solar cells [26]. One important advantage of these materials is their solution type processing techniques for fabrication that allows printable deposition of the films at room temperature and at atmospheric pressure in comparison to inorganic material deposition that usually requires high substrate temperature and complex high vacuum process. Recently with the introduction of organic materials and new technologies, new options have been studied for substitution of traditional TCOs to overcome some disadvantages as low transmission in blue region, high cost, complex high vacuum process, mechanical characteristics and scarcity. To achieve this here are some proposals: thin film grids [36],

highly carbon based materials [37] and organic polymers [38-40]. PEDOT:PSS has been one of the most investigated organic material as alternative to TCOs, the polymer has shown higher transparency and conductivity than traditional ITO contacts. Additionally, PEDOT:PSS can be deposited by dispersion in water which is compatible with large area, and flexible low-cost substrates [41].

In this section it has been studied the interface AZO/PEDOT:PSS to be applied on flexible photovoltaic solar cells. A thin film hybrid organic-inorganic photovoltaic structures based on hydrogenated silicon (Si:H) and poly(3,4ethylenedioxythiophene):poly(4-styrenesulfonate) (PEDOT:PSS) heterojunction deposited on different types of flexible substrates have been fabricated and investigated. Compatibility of the organic and inorganic materials and their technological regimes used for device fabrication has been demonstrated on flexible substrates. Morphological characteristics of transparent Al doped Zn:O (AZO) films deposited on substrates have been measured by atomic force microscopy. Electronic characteristics of the fabricated photovoltaic structures has been measured and analyzed for different thicknesses of the transparent electrodes and different substrate types.

The choice of an appropriate substrate is a crucial factor for hybrid flexible solar cells in the superstrate configuration (illumination through the substrate) because the substrate should be optically transparent and should withstand the processing temperature (in the range of 150-200º C) and the glow discharge conditions during deposition of semiconductor films in PECVD system. For this purpose, two types of flexible substrates - PEN and “Kapton” – have been selected. The first one, PEN (from “Tejin Inc.”), because of high optical transparency, and the second one, “Kapton”(from “DuPont, Inc. ”), because it can withstand glow discharge and high temperatures (∼450 °C) and can be suitable for space applications [1]. However, a main disadvantage of “Kapton” is a strong absorption of visible radiation. The sequence of deposited layers follows the structure presented schematically in Fig. 4.34.a.

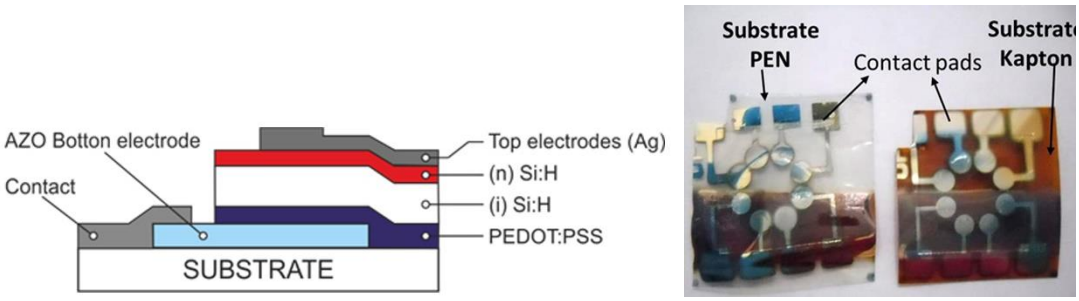

a) b)

Figure 4.34. a) Hybrid photovoltaic structure on flexible substrate based on Si:H and organic semiconductors PEDOT:PSS as p-type layer; b) photo of the fabricated structures on both PEN and Kapton substrates.

The device configuration studied is similar to a-Si:H based p-i-n structure where p-layer is substituted by organic semiconductor PEDOT:PSS. As the transparent electrode the Al:ZnO (AZO) films were deposited on top of flexible substrate by sputtering using a cluster multi chamber PECVD system from "MVSystem Inc." with different deposition times to obtain required thickness over different substrates. The AZO films were etched by hydrochloric acid to define the bottom electrode and cleaned with ultrasound baths in acetone and isopropyl alcohol, sequentially. The PEDOT:PSS blend mixtures were prepared from components purchased from "Ossila Ltd.". Prior to deposition, PEDOT:PSS mixture (1:6 weight ratio) was filtered with a PVDF (polyvinyleneflouride) filter with pore sizes of 0.45 µm. The PEDOT:PSS films with thickness of 250 nm were deposited by spin-coating at rotation speed of 2000 rpm in N_2 ambient.

The inorganic layers were deposited using a cluster multi chamber PECVD system from "MVSystem Inc." with RF discharge at frequency f = 13.56 MHz. To avoid cross contamination the doped and intrinsic layers were deposited in different chambers with transportation via vacuum camera. The intrinsic Si:H layers were deposited from an $10\%SiH_4 + 90\%H_2$ gas mixture at pressure P = 550 mTorr with deposition time selected to obtain required thickness. The 20 nm thick n-layers were deposited using $0.01\%PH_3 + 9.9\%SiH_4 + 90.09\% H_2$ gas mixtures at pressure P = 550 mTorr. The deposition temperature was fixed at T_d = 160° C and power at W = 3 Watt. All the gases used for deposited semiconductor films were semiconductor grade from “Matheson Inc.” The top contacts were deposited by evaporation or sputtering of Ag through a metal shadow mask with an area of

S_m=0.09 cm^2. Photos of the resulting hybrid structures on PEN and "Kapton" flexible substrates are shown in Fig 4.34.b.

For each substrate type, two devices AZO/ PEDOT:PSS/ (i) Si:H-(n)Si:H with different AZO electrode thickness have been fabricated: PEN/AZO(255nm)/ PEDOT:PSS/ (i) Si:H-(n)Si:H labeled as H42-2; PEN/AZO(510nm)/ PEDOT:PSS/ (i) Si:H-(n)Si:H labeled as H43-2; Kapton/AZO(255nm)/ PEDOT:PSS/ (i) Si:H-(n)Si:H labeled as H44-2; Kapton/AZO(510nm)/ PEDOT:PSS/ (i) Si:H-(n)Si:H labeled as H45-2. In addition, for comparison purposes, a reference AZO/ PEDOT:PSS/ (i) Si:H-(n)Si:H device on "Corning 1737" glass (labelled as H41-1) has been fabricated.

The cross-section scanning electron microscopy (SEM) image (from secondary electron regime) of the hybrid photovoltaic structure H44 is presented in Figure 4.35. It is seen, that AZO layer has well defined columnar structure with a column width of approximately W_{col} = 10-50 nm. PEDOT:PSS layer, deposited on AZO is rather inhomogeneous showing spherical inclusions, mainly at the PEDOT:PSS/a-Si boundary. It can be seen, however, that PEDOT layer "heals" rather rough top AZO surface, preparing smooth and planar surface for the deposition of intrinsic amorphous silicon layer. Thus, a-Si layer is deposited on better surface and looks rather homogeneous in thickness and structure (at the given resolution). Next, Ag layer, demonstrates well defined grain structure (with inverted pyramid form) and the grain size of around 50 - 150 nm. It is interesting to note, that the substrate defect (crack) is translated through the AZO layer (either during the deposition or due to the substrate bending) and this is interrupted due to the organic polymer layer prevents the further translation of the defect to the subsequent layers.

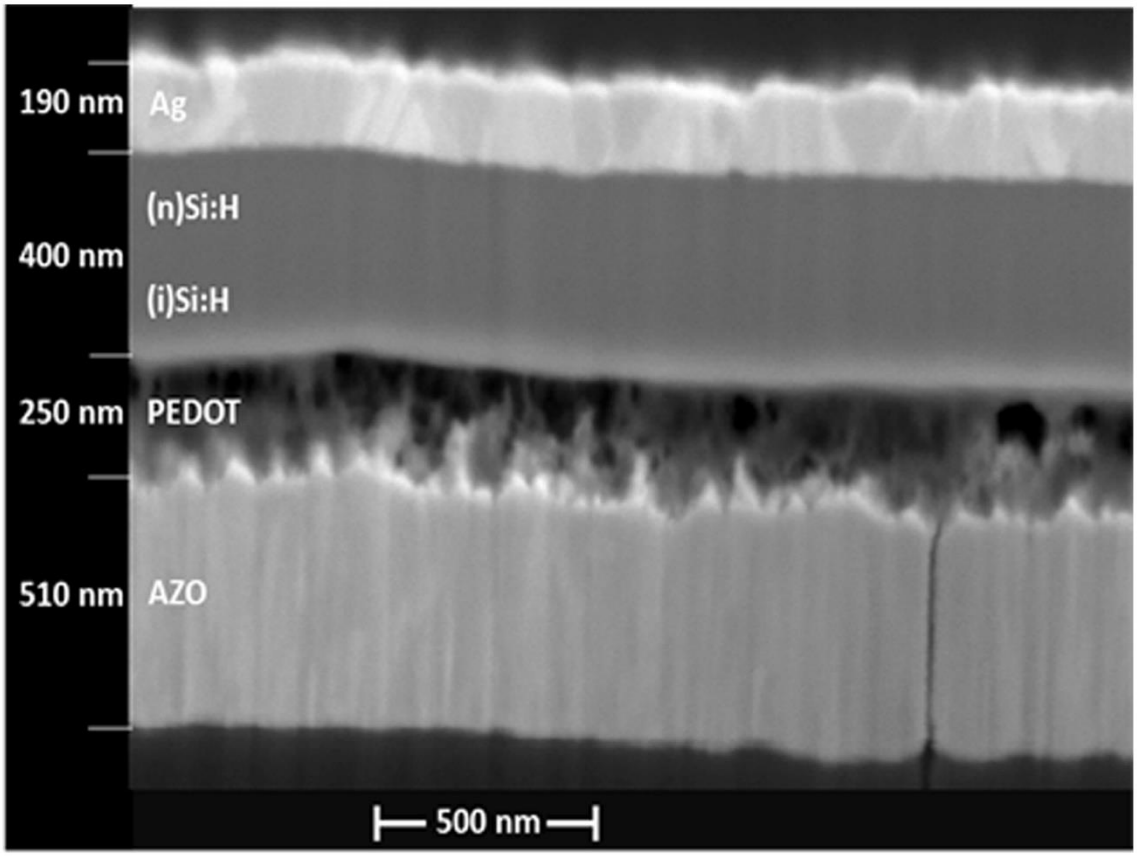

Figure 4.35. Cross-sectional SEM image of a representative device.

In order to study the electronic properties of our samples, the J(U) characteristics of the AZO/(p)PEDOT:PSS/(i)Si:H/(n)Si:H structures fabricated on PEN and "Kapton" substrates were measured (Fig. 4.36). For comparison purpose, the J(U) characteristics of cell prepared on glass substrates in the same technological run were measured in similar experimental conditions. For both substrates, the J–U curves of the devices measured under standard illumination (AM 1.5 I_0 = 100 mW/cm^2) from solar simulation are shown in Fig. 4.36.

Let us start analysis of the J(U) curves in Fig.4.36 with J_{SC}. The highest values are observed in the samples deposited on PEN substrates with minor difference between two samples due to different thickness of AZO layer. J_{SC} values in the samples fabricated on "Kapton" substrates are significantly less which is expected due to the poor transmission T(λ) in short wavelength region. Besides, electronic properties of junctions fabricated on different

substrates with different surface morphology could also be responsible for this differences (will be discussed later). As to the U_{OC} values all the structures have close values U_{OC} = 0.55 – 0.565 V excepting sample H42-2 with Uoc = 0.405 V.

It can be seen, that Jsc of the fabricated devices shows limitation of current in the range of U = 0.3 – Uoc (an S-shape of the Jsc(U) curve near U=Uoc). Therefore, low Fill Factor (FF) values (from 23 to 26 %) are observed in all the structures resulting from losses of current in these not optimized structures. Low FF often arises from parasitic shunt and series resistances and might be a signal of leakage through the organic layer or/and other semiconductor layers (see SEM image in Fig.4.35 for possible current channels). However, at present it is not clear yet if and how plasma could influence or induce such current channels.

It is observed, that performance characteristics of devices fabricated on PEN substrate are dependent on the thickness of AZO electrode. Two times increase of AZO electrode thickness results on the increase of current density J_{SC} from 3.21 mA/cm^2 to 9.79 mA/cm^2 and open circuit voltage U_{OC} from 405 mV to 565 mV, while fill factor FF remains almost unchanged. Thus, PCE increases from 0.31 to 1.3 %. It can be observed also, that characteristics of the devices fabricated on "Kapton" substrate, are independent on the AZO electrode thickness with a J_{SC} = 1.9 mA/cm^2 and U_{OC} = 550 mV.

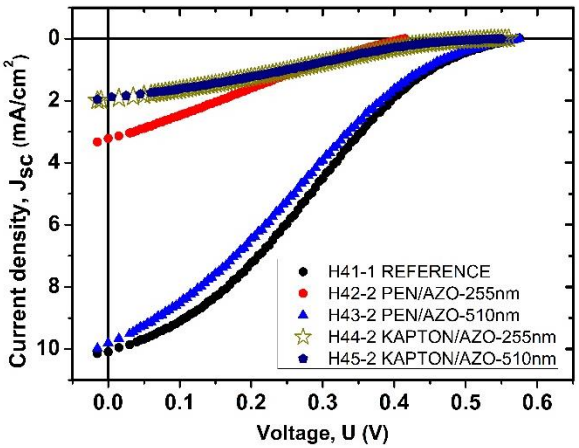

Figure 4.36.Current-voltage characteristics of hybrid photovoltaic structures: reference sample on "Corning 1737"glass (H41-1), AZO/ PEDOT:PSS/ (i) Si:H-(n)Si:H deposited on different substrates with different thickness of AZO electrodes: PEN/AZO(255nm)/PEDOT:PSS/ (i) Si:H-(n)Si:H (H42-2),

:PEN/AZO(510nm)/ PEDOT:PSS/ (i) Si:H-(n)Si:H (H43-2), Kapton/AZO(255nm)/PEDOT:PSS/ (i) Si:H-(n)Si:H (H44-2), Kapton/AZO(510nm)/ PEDOT:PSS/ (i) Si:H-(n)Si:H (H45-2).

The difference in J_{SC} in the studied structures can arise from the following factors: a) difference in the amount of photons absorbed in the structure due to the different spectral transmission T(λ) of the substrates in the range of λ= 400-600 nm; b) difference in electrical properties of the films grown on different substrates and junctions between them. However, most probably the joint effect of both a) and b) factors contributes to the device performance.

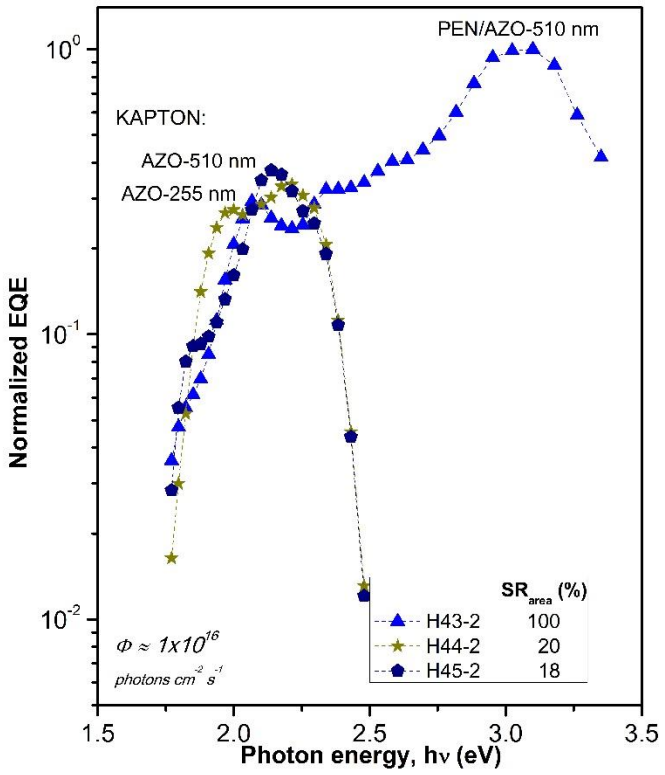

Figure 4.37. Spectral response of short circuit current density Jsc(hν) for hybrid photovoltaic structures 1) H43-2, 2)44-2, and 3)H45-2. Area under the curve (SR_{area}) is indicated for the samples taking H43-2 SR_{area} as reference.

Since we are interested in finding out what is the contribution of substrate on the electrical properties of the junction, in order to distinguish between these two contributions, spectral dependencies of short circuit current $J_{SC}(\lambda)$ in fabricated flexible photovoltaic structures were measured and analyzed. Spectral characteristics $J_{SC}(h\nu)$ in the range of λ from 354 to 1200 nm for three hybrid structures (H43-2, H44-2 and H45-2) are presented in Fig. 4.37. In $J_{SC}(h\nu)$ dependence three regions can be distinguished: 1) low photon energy region

(from hν = 1.8 – 2.2 eV) related to sub gap absorption, determined mainly by properties of the intrinsic layer, 2) intermediate region (from hν = 1.8 to 3.0eV) where the current is a result of contributions from entire PV structure and 3) high photon energy region (hν = 3.0 to 3.5 eV) where J_{SC} signal is mainly controlled by frontal interface properties. This last region and part of the region 2 are significantly shifted to low photon energy direction in the structure on "Kapton", because of its spectral transmission (Fig. 4.34.b). The loss of the short circuit current due to not optimal light harvesting in the structure on "Kapton" substrate can be estimated comparing the area under the corresponding curves of J_{SC} (λ) dependence (Fig. 4.37): it is 20 % in the structure H44-2 and 18 % in H45-2, where 100% corresponds to the H43-2 device. However, it is interesting to note, that short circuit current value Jsc(hv) in region 1 and part of the region 2 is higher (nearly by the factor of 2) in the hybrid structure fabricated on "Kapton" substrate, even though the PEN substrate provides better optical transmission in the same range of wavelength. We tried to compare the junctions themselves fabricated on PEN and "Kapton" substrates by means of recalculation of performance J(U) characteristics for the structures on "Kapton" reducing them to those on PEN substrates. The factor for this recalculation is obtained from spectral characteristics of the real devices illuminated by AM 1.5 light. This analysis reveals difference in the junctions mostly in short circuit current density (about 15% less for the junction on "Kapton" substrate) while open circuit voltage shows practically the same value. We believe that worse junction properties of "Kapton"- based device could arise from the morphological features of AZO surface deposited on "Kapton", characterized by higher roughness and by presence of sharp peaks of AZO, as shown by our AFM data. Such peaks can produce additional stress on the film grown on top of it and in this way contribute to the deterioration of electronic properties of junction. In addition, these peaks could be responsible for the creation of parasitic shunts across the junction deteriorating device performance.

CHAPTER 5

CONCLUSIONS

In this doctoral work four main research topics were investigated: A) Morphological influence of plastic substrates on p-i-n photovoltaic structure, B) Plasma treatment on plastic substrate to enhance adhesion of polymer and transparent conductive oxides thin films, C) Study of planarization of defects by polymer and inorganic thin films to reduce defect transition to p-i-n PV structures. At the end, the concepts developed were applied on functional flexible solar cells.

First, study of the evolution of morphological characteristics of Si:H p-i-n structures deposited by plasma on "corning" substrates showed that the behavior of average height, kurtosis and rms roughness parameters is very similar layer by layer. The maximum value of roughness is 3.14 nm for AZO layer and the lowest roughness value was 2.23 nm in the n-type layer. The highest average height has a magnitude of 12.81 nm (AZO layer) and the lowest height is 6.86 nm in the n layer. Based on the analysis of kurtosis, the grains of the resulting surfaces tend to take shape like a Gaussian. Analysis of the skewness values revealed that the surfaces of the layers demonstrated a comparable number of grains and pores. The weighted average values of diameters and average heights showed similar evolution behavior for 1-3 interfaces reaching maximum values on interface 4 (i-n interface). Aspect ratio showed maximum value on interface 4 (i-n interface) due to both high $<H>$ and lowest $<D_W>$ values, suggesting high height grains with relatively small diameters.

Material PEN is better as a substrate due to its better morphological evolution in the deposition of p-i-n structures (see table 4.12). In addition, PEN has an acceptable average transmittance value in the range 400-850 nm equal to 72.23% (see figure 4.12).

Teflon is an attractive material for further studies in photovoltaics because it has very high transmittance, 94.37% on average in the range of wavelengths between 400 and 850 nm (see Figure 4.12). Its low adhesion (see figure 4.17) and high density of defects (see table 4.5) is a disadvantage in the fabrication of photovoltaic devices but with that made in this

work it was demonstrated that it is possible to improve its adhesion by plasma processes (see figure 4.18) and its defect density can be reduced by means of planarization layers (see table 4.22).

Polyimide substrate initially showed the best morphological characteristics of the substrates (see table 4.10), however, it also showed the worst morphological evolution during the deposition of cells p-i-n (see table 4.12). Also, Polymide has the lowest transmittance (see figure 4.12), 55.84% between 400 and 850 nm.

Related to hybrid organic/inorganic p-i-n PV devices on flexible plastic substrates. The AFM results showed that surface morphological characteristics of AZO are affected by the substrates type, as well as, by the AZO thickness. SEM characterization has demonstrated the complexity of the material and interface of the structures, as well as an effect of "healing" of AZO surface by organic semiconductor. PV hybrid structure on PEN substrate showed the highest value of short circuit current density Jsc = 9.79 mA/cm^2, Uoc = 565 mV and PCE η = 1.3 %. This superior performance compared to that of the devices on "Kapton" substrate is mainly due to the wider optical transmission window of the PEN substrate. However, device diagnostics using the spectral dependence of the short circuit current has revealed that p-i-n junction of "Kapton"-based device itself provides about 15% less current that that on PEN-based device. All the materials, techniques and regimes used for fabrication proved to be compatible among each other allowing fabrication of multilayered device structures.

SCIENTIFIC PRODUCTION

Projects:

Member of **SENER-CONACYT No. 152244** project “Photovoltaic solar cells based in silicon-germanium deposited by plasma on flexible substrates”

Journal papers:

Mansurova, S.; Cosme, I.; Kosarev, A.; J. Olivares, A.; Ospina, C.; E. Martinez, H. AZO/PEDOT:PSS Polymer Frontal Interface Deposited on Flexible Substrates for a-Si:H Photovoltaic Applications. Polymers 2018, 10, 1068. https://doi.org/10.3390/polym10101068

International proceedings

1. Ospina, C., & Kosarev, A. (2014). Study of morphological characteristics of Si:H p-i-n structures deposited by plasma on plastic substrates. In *2014 11th International Conference on Electrical Engineering, Computing Science and Automatic Control, CCE 2014*. http://doi.org/10.1109/ICEEE.2014.6978308

2. Ospina, C., & Kosarev, A. (2015). Evolution of morphological characteristics of Si:H p-i-n structures deposited by plasma on corning substrates. In *2015 12th International Conference on Electrical Engineering, Computing Science and Automatic Control, CCE 2015*. http://doi.org/10.1109/ICEEE.2015.7357907

3. Martinez, H. E., Ospina, C., & Kosarev, A. (2015). Effect of hydrogen dilution on morphology and electronic properties of silicon-germanium films deposited by RF plasma discharge. In *2015 12th International Conference on Electrical Engineering, Computing Science and Automatic Control, CCE 2015*. http://doi.org/10.1109/ICEEE.2015.7357905

4. Olivares Vargas, A. J., Mansurova, S., Cosme, I., Kosarev, A., Ospina Ocampo, C. A., & Martínez Mateo, H. E. (**2017**). Hybrid solar cell base don a-Si/polymer flat heterojunction on flexible substrates. *SPIE Organic Photonics + Electronics, 2017, San Diego, California, United States*. Proc. SPIE 10363, Organic, Hybrid, and Perovskite Photovoltaics XVIII, 103632W (25 August 2017); doi: 10.1117/12.2274164

Conference presentations

1. Ospina, C.A., Kosarev, A., & Moreno, M. (2014). "Electronic characteristics of a-SiGe:H and pm-SiGe:H films deposited by Plasma Enhanced Chemical Vapor Deposition (PECVD) on plastic substrates". *9th International conference of Amorphous & Microcrystalline Semiconductors*, 7-10 July, 2014, St-Petersburg, Russia, ISSN 2218 2128.

2. Ospina, C., & Kosarev, A. (2015). "Morphological Characteristics of Si:H p-i-n Structures Deposited by PECVD on AZO/Glass Substrates". *8th International Conference on Surfaces, Materials and Vacuum*, 21-25 September, 2015, Puebla, Mexico. Proc. SEM-322

3. Ospina, C., Kosarev, A., Carrillo, J., Mansurova, S., Martínez, H., & Cosme, I. (**2017**). Study of light distribution in hybrid light emitting device. In 2017 *Mexican Optics and Photonics Meeting MOPM*. Puebla, Mexico.

4. Ospina, C., & Kosarev, A. (2014). "Study of morphological characteristics of Si:H p-i-n structures deposited by plasma on plastic substrates". *Electrical Engineering, Computing Science and Automatic Control, CCE.2014 11th International Conference on*. Ciudad del Carmen, Mexico.

5. Ospina, C., & Kosarev, A. (2015). "Evolution of morphological characteristics of Si:H p-i-n structures deposited by plasma on corning substrates". *Electrical Engineering, Computing Science and Automatic Control, CCE. 2015 12th International Conference on,* Ciudad de Mexico, Mexico.

List of figures

List of tables